CrystEngComm

RSC Publishing

PAPER

View Article Online
View Journal | View Issue

Cite this: *CrystEngComm*, 2013, **15**, 6845

Synthesis, topology and energy analysis of crystalline resorcinol-based oligophenylene molecules with various symmetries†

Clément Chaumont,[a] Pierre Mobian,*[a] Nathalie Kyritsakas[b] and Marc Henry*[a]

Received 30th April 2013,
Accepted 6th June 2013

DOI: 10.1039/c3ce40761f

www.rsc.org/crystengcomm

We describe the development of a set of highly symmetric multitopic oligophenylene molecules decorated with hydroxyl functions that are all derived from the resorcinol moiety. All these resorcinol-based oligophenylene self-assembled structures and the corresponding methoxy protected precursors were found to be highly crystalline materials, with two compounds giving rise to porous 3D-networks. The solid-state organisation of these molecules has been studied from three complementary viewpoints using metrical, topological and energy analyses. A quantitative interaction energy has been associated to each supramolecular interaction responsible for a given topology, even for the quite new and highly complex topologies evidenced. Thermal and luminescent properties of these materials have also been examined.

Introduction

In the field of materials science, crystalline porous coordination polymers occupy a particular place owing to their high potentialities in separation,[1] gas storage,[2] drug delivery,[3] catalysis,[4] or magnetism.[5] These Metal–Organic Frameworks (MOFs) are formed from metal ions or clusters connected with organic linkers. Focusing only on the role of these organic connectors, the major importance played by the ligand fine design to provide to the resulting networks structural rigidity and high porosity is well established. As a consequence, the very large and structurally diverse family of oligophenylene connectors have been shown to be particularly adapted to generate porous networks in the presence of metal ions.[6] Thereby, several families of oligophenylene ligands, depending on the nature of the coordinating groups that functionalise the rigid backbones, have been reported. These connectors are mainly dominated by molecules that incorporate rigid oligophenylene backbones bearing carboxylic acid,[7] phosphonic acid,[8] cyanide[9] or *N*-heterocyclic groups.[10] Besides the chemical nature of the groups attached to the rigid spacers, other factors linked to the ligands structural features have to be considered in order to predict, to govern or to understand the resulting MOF structure. For instance, within a specific class of ligands, by using the same inorganic node, it has been shown that the topology and the porosity of MOF systems are strongly influenced by the geometry and the size, respectively, of a given type of ligand.[11] Thereby, developing a novel family of connectors based on identical coordinating entities that are able to generate a library of compounds showing a high diversity in terms of symmetry and size is of fundamental importance.

In order to propose an alternative class of ligands to the existing systems that are able to form MOFs with oxophilic metals, we describe herein the development of a set of multitopic oligophenylene molecules decorated with hydroxyl functions and all derived from the resorcinol moiety. The choice of the resorcinol unit for creating a new family of oligophenylene connectors was motivated by the ideal 1,3 position of the hydroxyl functions on the phenyl ring to form extended networks in the presence of oxophilic metal ions.[12]

So, we establish here efficient synthetic protocols leading to linear and branched polytopic oligophenylene connectors displaying various symmetries and having, as a common feature, terminal resorcinol units. The members of this family are depicted in Fig. 1. Since a majority of ligands in the field of MOF chemistry are highly symmetrical compounds, we have chosen to report the preparation of highly symmetric molecules belonging to the D_{2h}, C_{2v}, D_{3h} and T_d group-points. The targeted resorcinol-based oligophenylene structures and the corresponding methoxy protected precursors were found to be highly crystalline materials and a particular focus has been devoted to understand their solid-state organisation from three complementary viewpoints:

(i) A local metrical analysis performed by looking at bond lengths and bond angles for both intramolecular and intermolecular interactions.

[a]*Laboratoire de Chimie Moléculaire de l'Etat Solide, UMR 7140, Université de Strasbourg, 67070 Strasbourg, France. E-mail: mobian@unistra.fr; henry@unistra.fr*
[b]*Laboratoire de Chimie de Coordination Organique, UMR 7140, Université de Strasbourg, 67070 Strasbourg, France*

† CCDC 934375–934378, 934380–934382, 934386 and 934387. For crystallographic data in CIF or other electronic format see DOI: 10.1039/c3ce40761f

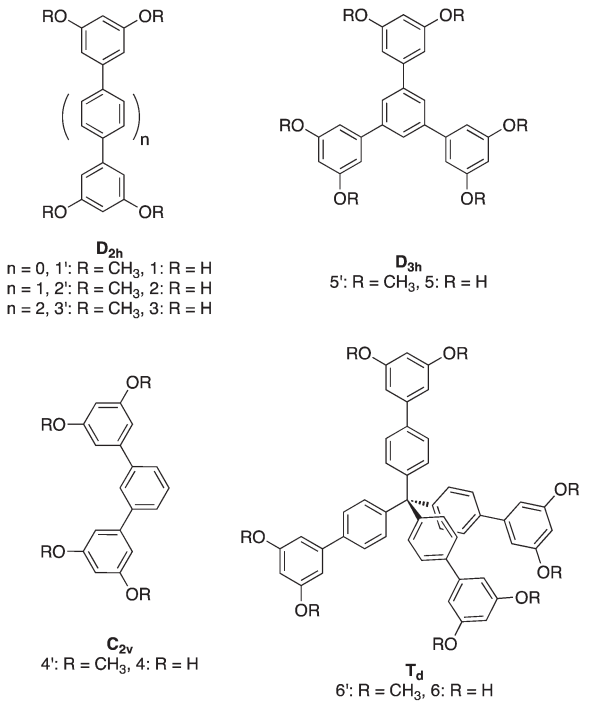

Fig. 1 The family of resorcinol-based oligophenylene molecules concerned by this study.

(ii) A global topological analysis performed using the TOPOS package[13] for determining the volume and mean radius of spherical domain (Rsd) of the molecular Voronoï-Dirichlet Polyhedron (MVDP), the coordination numbers and the point symbols of the underlying nets for both van der Waals and/or H-bond interactions. Let's recall that a point symbol lists the numbers and sizes of shortest circuits (closed chains of connected atoms) starting from every angle of every non-equivalent atom in the net.

(iii) An energetic analysis performed using the PACHA package[14] for retrieving quantitative energy values for all supramolecular interactions at work in these systems, as well as molecular dipole moments and packing energies.

A major finding of this systematic study is that two members were able to self-organise in the solid-state into porous networks. Furthermore, the thermal and luminescent properties of these solids have also been examined.

Results and discussion

Synthesis

Several synthetic methodologies have been developed to access oligophenylene structures; these include, for instance, reductive and oxidative coupling,[15] thermolysis and aromatisation of appropriate precursors,[16] and Diels–Alder cycloaddition.[17] Indeed, concerning the selected molecules, the application of transition-metal-catalysed aryl–aryl coupling reactions[18] looked the most adapted. Thus, the simple and straightforward two steps approach employed in the course of this study could be summarised as follows; the first step concerns the metallo-catalysed synthesis of the methoxy precursors starting from commercially or easily available molecules, whereas the second step deals with the cleavage of the methoxy groups leading to the target molecules. In most cases, the C–C formation was conducted by application of Suzuki–Miyaura reactions in the presence of the "classical" $Pd(PPh_3)_4$ catalyst.[19] It is worth noticing that compounds (**1**)[20] and (**5**)[21] are already known molecules. However, in the present work, we improve their accessibility and we characterised their crystalline solid-state organisations. Table 1 presents the procedures, the isolated yields and the precursors for the synthesis of compounds (**1′**) to (**6′**).

The synthesis of our library of compounds started with the preparation of (**1′**). Several synthetic methods have been envisaged and tested to obtain (**1′**): the Ullmann coupling, the Kumada–Corriu coupling or the palladium homo- and hetero-coupling reactions. The most efficient reaction to isolate (**1′**) is a homo-condensation of 3,5-dimethoxyphenylboronic acid mediated by the palladium(II) acetate, which allows the preparation of (**1′**) in a nearly quantitative yield. However, it appeared that the Suzuki–Miyaura reaction was the most applicable method for the synthesis of the other oligophenylene systems. All the target molecules, after a purification step over silica gel chromatography, were isolated with yields going from good to excellent. In particular, (**6′**) was obtained in an 80% yield, which is satisfactory if we consider that four C–C bonds were created in one step.

Next, the cleavage of the methoxy groups was conducted by using the classical BBr_3 reagent in anhydrous dichloromethane. In order to isolate the final compounds, two methods freed from the chromatography techniques were used. Since the conversions in most cases were quantitative, an extraction with diethylether of the hydrolysed crude medium was performed. A second option involved the basic treatment of the final reaction, followed by an acidification of the aqueous layer leading to the precipitation of the desired compounds, which were filtered-off. The deprotected molecules were obtained in yields varying from 93% to quantitative.

Table 1 Synthetic methodologies leading to the formation of (**1′–6′**). Experimental conditions: A: inert atmosphere, toluene/water/methanol, Na_2CO_3, $Pd(PPh_3)_4$ (5% mol), reflux; B: methanol, $Pd(OAc)_2$, room temperature, 5 hours; C: inert atmosphere, Mg, $Ni(PPh_3)_2Cl_2$, tetrahydrofuran, reflux overnight. Boronic acid/ester precursors: a: 3,5-dimethoxyphenylboronic acid, b: 4,4′-biphenylboronic acid bis(neopentyl)ester, c: 1-bromo-3,5-dimethoxybenzene, d: 1,4-dibromobenzene, e: 1,3,5-tribromobenzene, f: 1-bromo-4-[tris(4-bromophenyl)methyl] benzene

Experimental conditions	Boronic acid/ester precursors	Brominated precursors	Isolated yields	Compounds
A, 12 hours	a	c	95%	**1′**
B	a	—	98%	**1′**
C	—	c	75%	**1′**
A, 12 hours	a	d	82%	**2′**
A, 4 days	b	c	90%	**3′**
A, 24 hours	a	e	88%	**4′**
A, 12 hours	a	f	90%	**5′**
A, 4 days	a	g	80%	**6′**

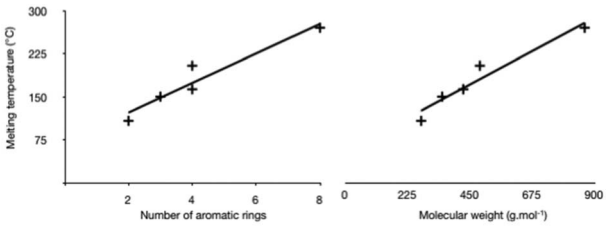

Fig. 2 Dependence of the melting point with the number of aromatic rings (left) or with the molecular weight (right) for derivatives (**1′–3′**) and (**5′–6′**).

Thermal stabilities

The methoxy derivatives (**1′–6′**) melted over a wide range of temperatures, between 87 °C and 270 °C, whereas the deprotected compounds (**1–6**) melted at above 300 °C evidencing much stronger intermolecular interactions.

If we except (**4′**), which melts at 87 °C, the melting points of (**1′–3′**) and (**5′–6′**) were correlated with the number of aromatic rings present in the backbone of the molecules (Fig. 2, left). An analogous tendency is observed if the melting points are plotted *versus* the molecular weights (Fig. 2, right). Independently to the molecular weight or the number of phenyl rings, the symmetry of the molecules seems also to influence the solid to liquid phase transition, since an unexpectedly low melting point for (**4′**) compared to the linear (**2′**) compound was found. Owing to the quite high melting points of (**1–6**), we turned to differential scanning calorimetry analysis (DSC) to evaluate the thermal properties of this family of compounds. The measurements were performed from 30 °C to 450 °C on the as-synthetised powders. The thermograms of (**1′–6′**) showed expected endotherms related to desolvation, vaporisation or fusion processes. Concerning (**1–6**), their thermograms were more complex compared to the protected derivatives. In particular, the DSC analysis of (**5**) and (**6**) clearly showed two exothermic processes occurring at 170 °C and 280 °C, respectively. As exothermic processes may occur from decomposition or bond breaking, the chemical integrities were verified for compounds (**5**) and (**6**) heated just above the observed exotherms. ^{1}H NMR and mass spectrometry as well as infrared analysis indicated that the chemical structures of (**5**) and (**6**) were unaffected by heating the samples at 180 °C and 280 °C, respectively.

Absorption and emission properties

Oligophenylene structures being known for their emission properties,[22] the absorption and the liquid and solid-state fluorescence measurements were performed for our series of derivatives. In general, the spectra are broad and structureless, with a notable exception concerning the fluorescence of compounds (**3**) and (**3′**). Table 2 lists the position of absorption and emission maxima. In solution, no marked differences of absorption and emission maxima between the non-linear derivatives with (**1**) or (**1′**) are noticed.

Furthermore, for a given member of the methoxy series, the wavelength absorption and the emission wavelength are highly comparable to those measured for the corresponding deprotected derivatives. A noticeable change of the absorption and emission properties arises when the number of aromatic rings increases within the series of linear molecules. For instance, a bathochromic shift for the absorption ($\Delta\lambda$ = 42 nm) is observed when going from (**1**) to (**3**). Such a shift to lower energy is a known common feature for *p*-oligophenylenes, which corresponds to the increase of the π-system.[23] Concerning the rather structured emission spectra of (**3**) and (**3′**), it is the signature of aromatic compounds that display a more planar configuration in the excited state than in the ground state.[24] The solid-state fluorescence spectra are presented in Fig. 3.

In general, for a given compound, the emission occurred at higher wavelength compared to the solution. Trends similar to those observed in tetrahydrofuran are found in the solid-state for the series of linear compounds. A particularly relevant observation concerns the large difference of emission wavelength between the two biphenyl derivatives (**1**) and (**1′**) ($\Delta\lambda \approx$ 19 nm), whereas in solution these two molecules exhibit almost the same emission maxima.

Table 2 Absorption and emission properties of (**1′–6′**) and (**1–6**) derivatives. (a) and (b) Solutions (10^{-5} mol L^{-1}) in tetrahydrofuran. (b) and (c) Excitation at λ = 246 nm

Compounds	Absorption[(a)] λ_{max} (nm)	Solution fluorescence[(b)] λ_{max} (nm)	Solid-state fluorescence[(c)] centered emission λ (nm)
1′	259	351	347
2′	290	354, 366	375
3′	301	356, 373	409
4′	255	350	348
5′	261	352	360
6′	266	351	361
1	260	358	366
2	294	371	394
3	302	373	395
4	256	354	368
5	264	352	364
6	267	353	369

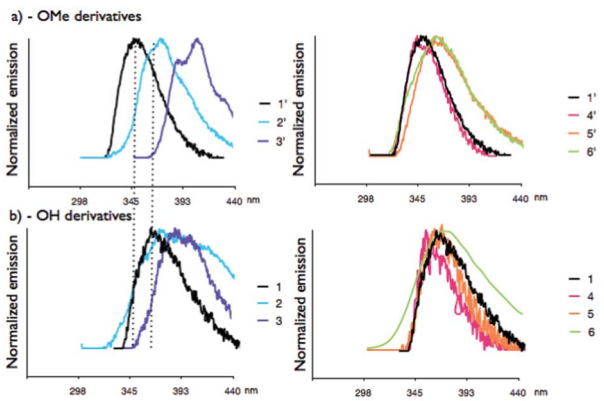

Fig. 3 The superimposed normalized solid-state fluorescence spectra in the –OMe derivatives (**1′–6′**) in (a) and the –OH derivatives (**1–6**) in (b). Excitation wavelength λ = 246 nm.

Solid-state structures

Solid-state structures of the linear oligophenylene derivatives (D_{2h}): (1′), (2′), (3′), (1) and (2). The compounds (**1′**), (**2′**) and (**3′**) are crystalline materials. Suitable single crystals for X-ray analysis were obtained in each case when *n*-pentane was allowed to diffuse in a dichloromethane solution of the oligophenylene molecule. The molecular structures of **1′**, **2′** and **3′** are presented in Fig. 4.

Concerning the conformations adopted by the phenyl rings in these three systems, one can notice in (**1′**) a synclinal arrangement of the two phenyl rings (measured torsion angle: 35°). When the molecular size increases, the two terminal phenyl rings adopt the same parallel orientation to one another but display a synclinal conformation when two consecutive phenyl rings are concerned. It is noteworthy that for (**3′**) the two central aromatic rings are coplanar. At the supramolecular level, the crystal organisation is driven essentially by π–π interactions. Compound (**1′**) is self-organised in staggered parallel bilayers, whereas the crystal organisation for (**2′**) and (**3′**) results from the repetition of antiparallel layers, as shown in Fig. 5.

MVDPs have been determined for the two crystallographically non-equivalent molecules of (**1′**) showing that both molecules have the same Rsd radius (4.35 Å) and volume (346 Å^3). The complete van der Waals topology corresponds to a 2-nodal 15,15-connected net with a new yet unknown topology having the point symbol $\{3^{39}.4^{56}.5^{10}\}_2$. This shows that each molecule is in van der Waals contact with 15 other molecules. After reduction of the two molecules to their respective centroids, a uninodal 10-connected net having the point symbol $\{3^{15}.4^{24}.5^6\}$ was evidenced corresponding to the **chb**/**CrB** topology (Fig. 6, left). Alternatively, these two inequivalent molecules were considered as a single dimeric supramolecular entity with a single centroid, leading to a uninodal 12-connected net having the point symbol $\{3^{24}.4^{36}.5^6\}$, corresponding to the **fcu**/**cubic** closest packing topology (Fig. 6, right).

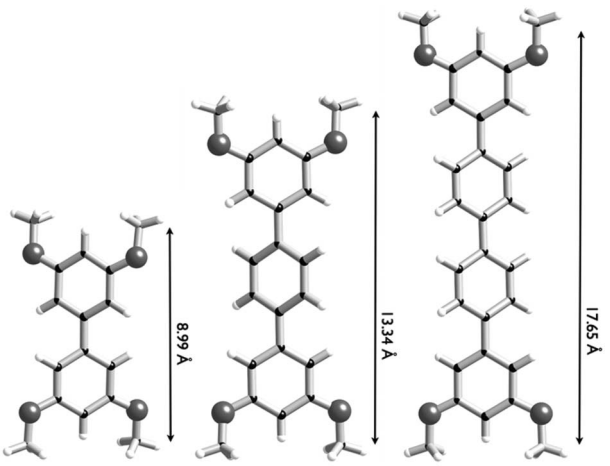

Fig. 4 Molecular structures of linear oligophenylenes (**1′**), (**2′**) and (**3′**). The distances indicated here correspond to those measured between two terminal aromatic hydrogen atoms.

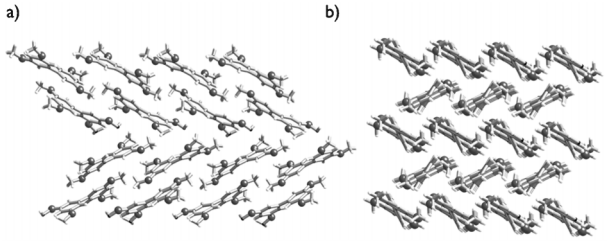

Fig. 5 Solid-state organisation of (**1′**) in (a) and (**2′**) in (b): (a) a view along the *y*-axis of the two antiparallel bilayers. (b) The solid-state arrangement of (**2′**) derived from the superimposed antiparallel layers. It is noteworthy that the crystal description for (**3′**) is analogous as the one made for (**2′**).

The molecular dipole moments of the two molecules were found to be 0.68 D and 0.73 D, leading to a packing energy of −27 kJ mol^{-1}. As these molecules form a 15-connected net, the average interaction energy per bond is −27/15 = −1.8 kJ mol^{-1}, demonstrating that this net cannot be based on purely van der Waals stacking of the molecular entities. Taking account the existence of π–π interactions evidenced in the metrical analysis in the form of dimers, the π–π bond energy may be evaluated as −27/2 = −14 kJ mol^{-1}, in good agreement with theoretical computations that predict values ranging from 10 kJ mol^{-1} up to 15 kJ mol^{-1} for this kind of interaction.[25]

From their respectives MVDPs, (**2′**) and (**3′**) were found to have a Rsd radius of 4.73 Å (**2′**) and 5.04 Å (**3′**) corresponding to molecular volumes of 442 Å^3 (**2′**) and 536 Å^3 (**3′**). The topology of the complete van der Waals net of both molecules corresponds to a uninodal 14-connected net with a **bcu-x** topology having the point symbol $\{3^{36}.4^{48}.5^7\}$. This shows that each molecule is in van der Waals contact with 14 other molecules. Reducing (**2′**) to its centroid leads to a uninodal 10-connected net having the point symbol $\{3^{12}.4^{28}.5^5\}$, corresponding to the **bct** (body-centered tetragonal) topology (Fig. 7, left). For (**3′**) an uninodal 6-connected net was evidenced having the point symbol $\{4^{12}.6^3\}$, corresponding to the **pcu** topology (Fig. 7, right). Both (**2′**) and (**3′**) have a zero molecular dipole moment, explaining the much reduced PE = −20 kJ mol^{-1} relative to the polar molecule (**1′**). The average

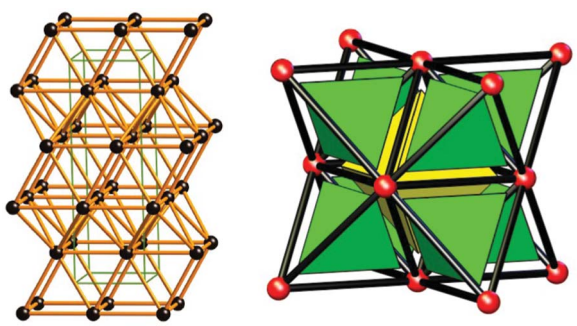

Fig. 6 Topological organisation of (**1′**) viewed as a uninodal 10-connected net displaying the **chb**/**CrB** topology based on two crystallographically non-equivalent molecules (left) or as a uninodal 12-connected net displaying the **fcu**/**ccp** topology based on stacking of molecular dimers (right).

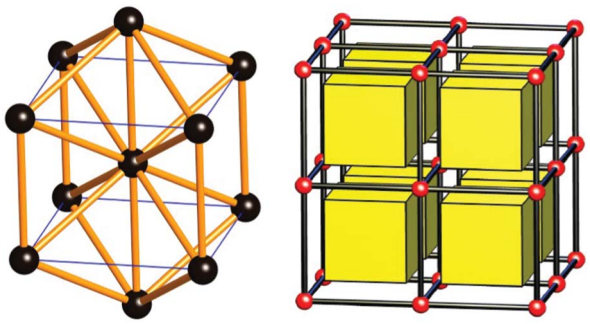

Fig. 7 The topological organisation of (**2′**) viewed as a uninodal 10-connected net displaying the body-centered tetragonal (**bct**) topology (left) and the topological organisation of (**3′**) viewed as a uninodal 6-connected net displaying the primitive cubic (**pcu**) topology (right).

interaction energy per molecule in these two 14-connected nets was $-20/14 = -1.4$ kJ mol^{-1}, demonstrating the purely van der Waals nature of these nets.

Concerning the solid-state characterisation of the deprotected linear compounds, we were able to obtain X-ray quality crystals for (**1**) and (**2**) by slow evaporation of an ethanol solution of (**1**) and by diffusion of *n*-hexane in an ethyl acetate solution of (**2**). Despite the fact that in both cases hydrogen bonds are the key interaction to govern the crystalline supramolecular organisation, the crystal descriptions are very different. Compound (**1**) crystallises in a $P\bar{1}$ space group. The molecular structure shows that the two aromatic rings adopt a coplanar arrangement. Analysis of the molecular packing of (**1**) reveals that one molecule of (**1**) co-crystallises with two equivalent water molecules. Each water molecule behaves at the same time as a hydrogen bond donor and acceptor with neighbouring OH groups, as shown in Fig. 8a. The closest O3···OH distances are found to be 2.7745(33) Å for O3···O1 and 2.7211(19) Å for O3···O2. Interestingly, O2 also interacts with a neighbouring phenol group through a hydrogen bond, the closest O2···O2 intermolecular distance is 2.7136(40) Å (not shown on the figure). Thus, an expansion of the motif shown in Fig. 8a through these two types of hydrogen bond leads to a two-dimensional sheet (Fig. 8b). Finally, interplanar hydrogen bonds between the water molecules and the O1 oxygen atoms are responsible for the three-dimensional arrangement in the form of stacked layers (interlayer O3···O1 distance: 2.8756(33) Å). The view along the *x* axis in Fig. 8c focuses on this interaction.

From its MVDP, (**1**) has a Rsd radius of 3.73 Å with a volume of 218 Å^3. The topology of the complete van der Waals net of (**1**) corresponds to a 2-nodal (5,18)-connected net characterized by a new yet unknown topology having the point symbol $\{3^5.4\}_2\{3^{30}.4^{70}.5^{45}.6^7.7\}$. Each molecule (**1**) has 10 van der Waals contacts with other (**1**) molecules and 8 other contacts with water molecules. Considering only H-bonding interactions involving (**1**) and the two water molecules leads to a net of known topology (**tfz-d**, UO_3) based on a 2-nodal (3,8)-connected net having the point symbol $\{4^3\}_2\{4^6.6^{18}.8^4\}$. However, it is worth noticing that TOPOS was not able to build a MVDP for the water molecule owing to the rather unusual disposition of its H-atoms with very short H···H contacts (0.9 Å) along the direction of the H-bonding. The X-ray coordinates for H-atoms H1, H2A, H3A and H3B were thus discarded and re-determined through minimisation of the partial electrostatic energy of the crystal using PACHA. As it was not possible to decrease the lattice energy by considering a unit-cell of $P\bar{1}$ symmetry with 5 adjustable torsion angles, the space group symmetry was lowered to *P*1 with 10 variable torsion angles. Then, it was possible to find a significantly more stable configuration for the overall H-bond pattern (-1035.1 kJ mol^{-1} *versus* -946.0 kJ mol^{-1} for the original CIF file) without any unrealistically short H···H contacts and where each water molecule forms, as expected, 4 hydrogen bonds (instead of the three in the original CIF file). With this new optimized structure, TOPOS was able to build MVDPs for (**1**) and water, changing the topological radius of (**1**) to 3.83 Å with a larger volume of 235 Å^3. The topology of the complete van der Waals was now a 3-nodal (4,6,22)-connected net with a new yet unknown topology having the point symbol $\{3^5.4\}\{3^{11}.4^4\}\{3^{50}.4^{121}.5^{59}.6\}$. Each molecule of (**1**) has 12 van der Waals contacts with other (**1**) molecules and 10 other contacts with water molecules. Considering only H-bonding interactions, we got a new yet unknown topology based on a 2-nodal (4,8)-connected net having the point symbol $\{4^5.6\}_2\{4^{10}.6^{14}.8^4\}$. For this optimised structure, water molecules were found to act as extremely weak electron donors with an overall polarity $(\mathbf{1})^{-0.01}(H_2O)_2^{+0.005}$. (**1**) was found to be a significantly polar molecule with a molecular dipole moment μ = 1.1 D. The overall H-bonding packing energy was quite large:

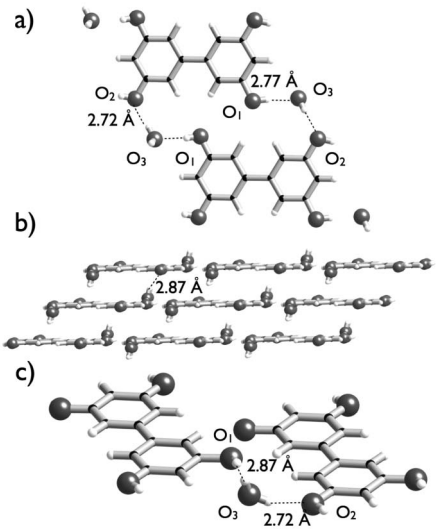

Fig. 8 Molecular recognition between (**1**) and the water molecules in the crystal structure of (**1**) is shown in (a). A view along the *z* axis of the three-dimensional arrangement of molecules in the crystal structure of (**1**), in the form of stacked layers is shown in (b). The dotted lines represent the hydrogen bonds responsible for the crystal packing. A view along the *x* axis highlighting the interlayer hydrogen bond between O1 and a water molecule is shown in (c). The water molecule and the (**1**) molecule with the oxygen atoms marked as O3 and O2, respectively, belong to the layer. It should be noted in (a) that O2 is also involved in an intermolecular hydrogen bond with a neighbouring (**1**) molecule (O2···O2 = 2.7136(40) Å). This interaction is not detailed on the figure.

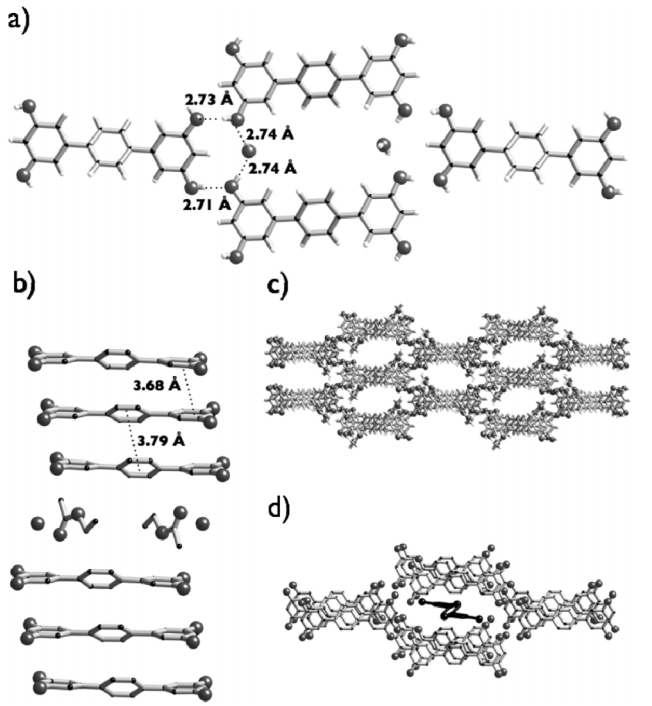

Fig. 9 A view along the *x*-axis of a tetrameric motif composed by four (**2**) molecules and two water molecules is shown in (a). A hydrogen bonded recognition motif composed by five oxygen atoms is highlighted using dotted lines. A view along the *y*-axis of trimeric columnar assemblies sandwiching a layer composed by two water molecules and two ethylacetate molecules is shown in (b). The hydrogen atoms have been omitted for clarity. A view along the *y*-axis of the network partially represented evidencing a honey-comb like structure is shown in (c). A perspective view evidencing the presence of threaded (**2**) molecules within the honey-comb network is shown in (d).

PE = −153 kJ mol^{-1}. As (**1**) is involved in 8 H-bonds and each water molecule is involved in 4 H-bonds, this packing energy corresponds to (8 + 2 × 4)/2 = 8 H-bonds, *i.e.* to an average bond energy E_{HB} = −153/8 = −19 kJ mol^{-1}, a value typical of O–H···O bonding between neutral molecules. Moreover, by removing the water dimers, leaving a H-bonded net of (**1**), it was possible to figure out the energies of the three kinds of H-bonding interactions at work in this net: $E_{HB}(H_2O\cdots H_2O)$ = −31 kJ mol^{-1}; $E_{HB}[H_2O\cdots(\mathbf{1})]$ = −27 kJ mol^{-1} and $E_{HB}[(\mathbf{1})\cdots(\mathbf{1})]$ = −10 kJ mol^{-1}. As expected, the H-bond energy between phenolic moieties is significantly less stabilizing than that involving water molecules.

Next, the solid-state organisation of (**2**) was examined. Compound (**2**) crystallises in a $P2_1/c$ space group. Four molecules of (**2**) crystallise with two ethylacetate molecules and seven water molecules. The central ring adopts, compared to the two terminal resorcinol units, a synclinal conformation (measured torsion angle: 32°). In this structure, the role of the crystallisation solvent that co-crystallises with (**2**) is essential to explain the crystal cohesion. The detailed analysis of the packing reveals that (**2**) forms first a layer, which could be decomposed as an infinite assembly of the tetrameric motif shown in Fig. 9a. The key feature explaining the formation of this two-dimensional sheet concerns the presence of a bridging water molecule interacting through two hydrogen bonds with two adjacent phenol groups, belonging to two different molecules. Thus, each of these two OH moieties is hydrogen bonded with a neighbouring resorcinol unit, leading to a five oxygen centre recognition motif as shown in Fig. 9a. Looking at the three-dimensional arrangement, it appears that each molecule is surrounded on each side by another oligophenylene derivative, leading to columnar assemblies that are governed by π-stacked interactions (phenyl rings centroid distances are measured at around 3.7 Å, see Fig. 9b). Thus, two of these columnar assemblies sandwiches a layer containing two ethylacetate molecules and two water molecules. At this stage, the resulting network obtained from the repetition of the motif described in Fig. 9b could be regarded as a honeycomb-like structure (Fig. 9c). Finally, the resulting cavities are fitted by threaded (**2**)-molecules (Fig. 9d), thereby the solid-state organisation of (**2**) is related as a pseudorotaxane type structure,[26] as it is schematically represented in Scheme 1.

From their respective MVDPs, the three non-equivalent molecules of (**2**) have Rsd radii of 4.38 Å (**2**a), 4.37 Å (**2**b) and 4.28 Å (**2**c), with a volume of 353, 349 and 328 Å^3, respectively. The topology of the complete van der Waals net of the crystal is a completely new yet unknown 8-nodal (6,6,8,8,11,21,24,28)-connected net having the stoichiometry $(6\text{-c})_2(6\text{-c})_2(8\text{-c})_2(8\text{-c})_2(11\text{-c})_2(21\text{-c})_2(24\text{-c})(28\text{-c})_2$.

Molecule (**2**a) is the node of a 21-connected net having the point symbol $\{3^{47}.4^{99}.5^{59}.6^5\}$, with nine contacts with other (**2**)-molecules, six contacts with water molecules, four contacts with CH_3COOEt molecules and two contacts with a void of radius 2.23 Å displaying a volume of 46 Å^3, occupied by a single isolated O-atom O13. Molecule (**2**b) is the node of a 28-connected net having the point symbol $\{3^{62}.4^{180}.5^{127}.6^9\}$, characterised by fourteen contacts with other (**2**)-molecules and fourteen contacts with water molecules. Molecule (**2**c) is the node of a 24-connected net having the point symbol $\{3^{58}.4^{106}.5^{89}.6^{23}\}$, characterised by ten contacts with other (**2**)-molecules, eight contacts with water molecules, four contacts with CH_3COOEt molecules and two contacts with the void. CH_3COOEt molecule is the node of the 11-connected net having the point symbol $\{3^{20}.4^{27}.5^8\}$ characterised by six contacts with (**2**)-molecules, three contacts with the void, and one contact with a water molecule and another CH_3COOEt

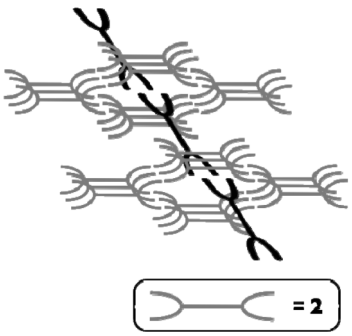

Scheme 1 Schematic representation of the pseudorotaxane type structure of (**2**) reflecting a not perfect alignment of the threaded molecules within the structure (represented in black).

molecules. The void is the node of one of the two 8-connected nets with three contacts with either (**2**) or CH_3COOEt molecules and two contacts with water molecules having a point symbol $\{3^{11}.4^{15}.5^2\}$. The node of the other 8-connected net, having a $\{3^{13}.4^{14}.5\}$ point symbol, is the O11-based water molecule having six contacts with (**2**)-molecules and two contacts with the void. Finally, the water molecules based on atoms O12 and O14 form the nodes of two 6-connected nets sharing the same point symbol $\{3^{10}.4^5\}$. The O12-based water molecule has six contacts with (**2**)-molecules whereas the O14-based one has five contacts with (**2**)-molecules and one contact with a CH_3COOEt molecule.

This very complex topology may be further simplified by considering only H-bonding interactions between molecular tectons, generating another completely new 7-nodal (1,4,4,4,6,8,8)-connected net displaying the stoichiometry (1-c)$_2$(4-c)$_2$(4-c)$_2$(4-c)$_2$(6-c)(8-c)$_2$(8-c).

Molecule (**2a**) is now the node of a double 8-connected net having the point symbol $\{4^{14}.6^{11}.7^2.8\}$ and is H-bonded to itself through four H-bonds and also to two O11–water (O3, O4) and two O14–water (O1, O2) molecules. Molecule (**2b**) is the node of the other 8-connected net having a point symbol $\{4^{14}.6^{12}.7^2\}$ and is also H-bonded to itself through four H-bonds, with the other four bonds involving the O12–water. Molecule (**2c**) is the node of a 6-connected net having the point symbol $\{4^2.5^2.7^2.8^9\}$ and is not H-bonded to itself, being rather engaged into one H-bond with the O14–water through each O7-atom and in two H-bonds with the O11–water and O12–water through each O8-atom. Each water molecule is the node of a 4-connected net but with different point symbols. The point symbol for the O11–water node is $\{4^3\}$ with one H-bond with CH_3COOEt, two H-bonds with (**2a**) and one H-bond with (**2c**). The point symbol for the O12–water node is $\{4.5^4.6\}$, with one H-bond with the O14–water, two H-bonds with (**2b**) and one H-bond with (**2c**). The point symbol for the O14–water node is $\{4^3.5.6^2\}$, with one H-bond with the O12–water, two H-bonds with (**2a**) and one H-bond with (**2c**). Finally, the CH_3COOEt molecule H-bonded to the O11–water molecule is the node of a 1-connected net having the point symbol {0}, meaning that it corresponds to a dead-end for the H-bonding networking interactions.

The next step was to characterise the overall electronic density partition as well as the relative magnitudes of each networking interaction within this very interesting new highly complex net. Partial charges analysis confirms the molecular nature of this framework with the following charge partition:

$$(\mathbf{2a})_2{}^{-0.00}(\mathbf{2b})^{+0.06}(\mathbf{2c})^{-0.08}(CH_3COOEt)_2{}^{-0.02}$$

$$(wO11)_2{}^{+0.01}(wO12)_2{}^{+0.015}(wO14)_2{}^{-0.02}$$

It is worth noting that (**2b**) and (**2c**) have a null dipolar moment, whereas that of (**2b**) was found to be μ = 0.13 D. The overall packing energy corresponding to a $(\mathbf{2})_2{\cdot}(H_2O)_3{\cdot}(CH_3COOEt)$ stoichiometry was found to be: PE = −430 kJ mol^{-1}. The largest stabilizing H-bond energy was that involving the non-networking CH_3COOEt molecules (μ = 2.03 D) with E_{HB}(CH_3COOEt···wO11) = −37 kJ mol^{-1}. Next comes the H-bonding interaction between (**2**) and water molecules, which may be split into two groups. One with an energy quite similar to that involving CH_3COOEt molecules with values: E_{HB}(**2c**···wO12) = −36 kJ mol^{-1} and E_{HB}(**2b**···wO12) = E_{HB}(**2c**···wO11) = −34 kJ mol^{-1}. Then another less stabilizing group with E_{HB}(**2a**···wO14) = −30 kJ mol^{-1}, E_{HB}(**2a**···wO11) = −27 kJ mol^{-1} and E_{HB}(**2c**···wO14) = −25 kJ mol^{-1}. The H-bond energy between the two water molecules was quite standard with E_{HB}(wO12···wO14) = −21 kJ mol^{-1}. Finally, the less stabilizing H-bond energies were those linking the (**2**)-molecules together with E_{HB}(**2b**···**2b**) = −18 kJ mol^{-1} and E_{HB}(**2a**···**2a**) = −17 kJ mol^{-1}. Summing together all these H-bonding interactions according to the observed topology then leads to an overall H-bond packing energy of PE_{HB} = −389 kJ mol^{-1}. Comparing this value to the total packing energy leaves −42 kJ mol^{-1} of stabilizing energy through van der Waals packing. From the van der Waals topology outlined above, this corresponds to 52 van der Waals interactions, *i.e.* to an average energy $<E_{vdW}>$ = −0.8 kJ mol^{-1} for each van der Waals interaction. As this is of the right order of magnitude for this kind of interaction, it may be safely concluded that about 90% of the packing energy may be associated with highly specific hydrogen bonding interactions whereas the other 10% comes from non-specific van der Waals stacking between molecular quasi-neutral tectons.

Solid-state structures of the D_{3h} and C_{2v} oligophenylene derivatives: 4′, 5′ and 5. The structures of (**4′**) and (**5′**) were both resolved from crystals obtained when *n*-pentane was allowed to diffuse into dichloromethane solutions of the oligophenylene derivatives. These two compounds crystallise in the same space group ($P\bar{1}$).

In the molecular crystal structure of (**4′**), the two terminal phenyl rings adopt, respectively, a synperiplanar and a synclinal conformation in relation to the central phenyl ring (Fig. 10). At the supramolecular level, the structure of (**4′**) could be regarded as an infinite self-association of molecules into chains. According to the structure, the centroid phenyl ring distance between the two aromatic moieties in these chains is evaluated at 3.49 Å. From its MVDP, the (**4′**)-molecule has a topological radius of 4.73 Å for a volume of 444 Å^3. The complete van der Waals topology corresponds to a new original uninodal 18-connected net having the point symbol $\{3^{60}.4^{88}.5^5\}$, meaning that each molecule is in van der Waals contact with 18 other molecules. The molecular dipole moments of (**4′**)-molecules were found to be 1.23 D, leading to a packing energy of −23 kJ mol^{-1}. As these molecules form an 18-connected net, the average interaction energy per van der Waals bond is −23/18 = −1.3 kJ mol^{-1}. This rather low value may be associated to weak CH···O hydrogen bonds characterized by an average HC···O distance of 3.8497(23) Å.

Concerning the (**5′**) crystal, the crystal organisation is derived from supramolecular dimers where two (**5′**)-molecules stack *via* π–π-interactions with a staggered conformation (centroid central phenyl ring distance: 3.56 Å) as shown Fig. 11a. These dimers further interact again *via* π–π-interactions with neighbouring dimers to form supramolecular chains and sheets that are interdigitated, as attested in the crystal view in Fig. 11b. From its MVDP the (**5′**)-molecule has a Rsd radius of 5.33 Å for a volume of 635 Å^3. The complete van der Waals topology corresponds to a new original uninodal 19-

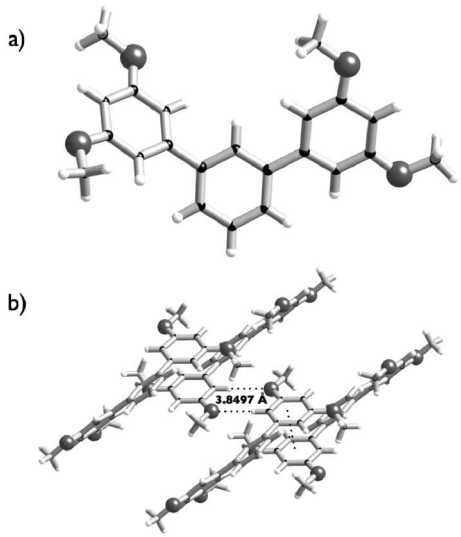

Fig. 10 The molecular structure of (**4′**) is shown in (a). An illustration of the solid-state supramolecular organisation of (**4′**) is shown in (b). A distance of 3.49 Å between two centroid phenyl rings (represented as a dotted line) is estimated from the structure evidencing π–π-interaction leading to the formation of a supramolecular dimer. Two dimeric motifs are self-associated *via* CH···O contacts as illustrated by the two dotted lines joining the hydrogen and the oxygen atoms (average measured HC···O distances: 3.8497(23) Å).

connected net having the point symbol $\{3^{63}.4^{102}.5^{6}\}$, meaning that each molecule is in van der Waals contact with 19 other molecules. The molecular dipole moments of (**5′**)-molecules were found to be 1.70 D, leading to a packing energy of −45 kJ mol^{-1}. As these molecules form a 19-connected net, the average interaction energy per van der Waals bond is −45/19 = −2.4 kJ mol^{-1}. As this value is a little bit too high for pure van der Waals interactions, a (**5′**)-dimer was generated allowing us to derive an interaction energy E_{int}(**5′**···**5′**) = −17 kJ mol^{-1}, which is more in line with aromatic π–π-stacking. Linking dimers into chains, chains into layers and stacking layers together then leads to E_{int}(dim···dim) = −11 kJ mol^{-1}, E_{int}(chain···chain) = −10 kJ mol^{-1} and E_{int}(layer···layer) = −11 kJ mol^{-1}.

Single crystals of (**5**) were produced when an acetone (solvent)/chloroform (counter-solvent) system was used. Fig. 12 partially represents the supramolecular organisation of the crystal. Again, in the crystal, π-stacked interactions generate columnar assemblies (not shown on the figure). Perpendicularly to this 1D network, (**5**) is involved in a hydrogen bonded network. Fig. 12 highlights the organisation of four (**5**)-molecules in the crystal through four hydrogen bonds leading to pseudo-channels filled with acetone and water molecules (not shown on the figure). Molecules of (**5**) have a Rsd radius of 4.74 Å for a volume of 446 Å^3. The topology of the complete van der Waals net of the crystal is again a new unknown 4-nodal (7,8,12,26)-connected net having the stoichiometry (7-c)(8-c)(12-c)(26-c). (**5**) is the node of a 26-connected net having the point symbol $\{3^{73}.4^{159}.5^{91}.6^{2}\}$, with eleven contacts with other (**5**)-molecules, five contacts with a water molecule, five contacts with a first acetone molecule AC1 and five contacts with another acetone molecule AC2. Acetone molecule AC2 is the node of a 12-connected net having the point symbol $\{3^{27}.4^{34}.5^{5}\}$, characterised by five contacts with (**5**)-molecules, three contacts with AC1, two contacts with AC2 and two contacts with a water molecule. Acetone molecule AC1 is the node of an 8-connected net having the point symbol $\{3^{17}.4^{11}\}$, characterised by five contacts with (**5**)-molecules and three contacts with acetone molecule AC2. Finally water is the node of a 7-connected net having the point symbol $\{3^{15}.4^{6}\}$, characterised by five contacts with (**5**)-molecules and two contacts with acetone molecule AC2. As before, this topology may be further simplified by considering only H-bond interactions between molecular tectons, generating another new 4-nodal (1,1,3,9)-connected net displaying the stoichiometry (1-c)(1-c)(3-c)(9-c).

Molecule (**5**) is now the node of a 9-connected net having the point symbol $\{4^{13}.6^{14}.8\}$ and is H-bonded to itself through six H-bonds, to water molecules with two H-bonds and to the acetone molecule AC1 with one H-bond. The point symbol for the water node of the 3-connected net is {4} with two H-bonds with (**5**) and one H-bond with the acetone molecule AC2. Finally, both the acetone molecules AC1, which is H-bonded to (**5**) and AC2, which is H-bonded to water, are the nodes of a two 1-connected net having the point symbol {0} and should thus be considered as dead-ends for H-bonding networking interactions.

Partial charges analysis confirms the molecular nature of this framework with the following charge partition:

$$(\mathbf{5})^{-0.11}(H_2O)^{+0.03}(AC1)^{+0.03}(AC2)^{+0.04}$$

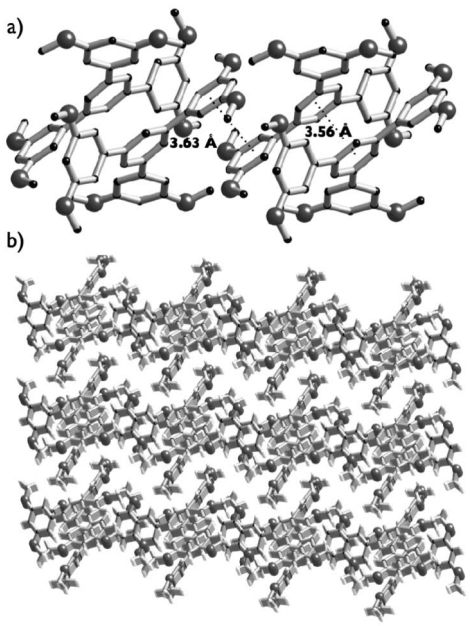

Fig. 11 A view of two (**5′**)-dimers self-associated *via* π-stacked interactions is shown in (a). These dimers, where a staggered conformation is observed, result from an aromatic stacking between the central phenyl rings of the molecules. The hydrogen atoms have been omitted for clarity. A view of the interdigitated sheets that compose the crystal structure is shown in (b).

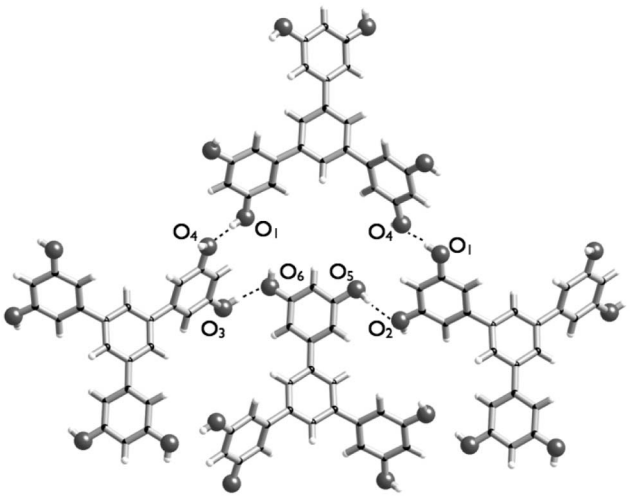

Fig. 12 Hydrogen bonding network in the crystal of 5. d(O3···O6) = 2.7200(16) Å, d(O5···O2) = 2.8714(17) Å, d(O1···O4) = 2.6708(19) Å.

The molecular dipolar moment of (**5**) was found to be $\mu = 0.4$ D, with an overall packing energy corresponding to a (**5**)·(H_2O)·(Me_2CO)$_2$ stoichiometry that was found to be: PE = -299 kJ mol^{-1}. The largest stabilizing H-bond energy was involving the non-networking acetone AC1 with E_{HB}(**5**···AC1) = -47 kJ mol^{-1}. Next, comes the H-bonding interaction between (**5**) and the water molecule: E_{HB}(**5**···H_2O) = -35 kJ mol^{-1}. The H-bond energy between the water molecules and the other non-networking acetone molecule was E_{HB}(wO12···wO14) = -26 kJ mol^{-1}. Finally, the less stabilizing H-bond energies were those linking (**5**)-molecules together with E_{HB}(**5**···**5**) = -17 kJ mol^{-1}. Summing together all these H-bonding interactions according to the topology then leads to an overall H-bond packing energy PE_{HB} = -276 kJ mol^{-1}. Comparing this value to the total packing energy leaves -23 kJ mol^{-1} of stabilizing energy through van der Waals packing. From the van der Waals topology outlined above, this corresponds to 27 van der Waals interactions, *i.e.* to an average energy $<E_{vdW}>$ = -0.9 kJ mol^{-1} for each van der Waals interaction. Consequently, it may be safely concluded that about 92% of the packing energy may be associated with highly specific hydrogen bonding interactions whereas the other 8% comes from non-specific van der Waals stacking between molecular quasi-neutral tectons.

Solid-state structures of the tetraphenylmethane derivatives: 6 and 6′. In the field of crystal engineering, molecules based on a tetraphenylmethane backbone are particularly attractive building blocks since these compounds usually self-assemble into crystalline networks, encapsulating guest molecules in large channels.

A survey of the 1.1.1 release of the Cambridge Structural Database reveals that about forty tetraphenylmethane-based molecules displaying a T_d symmetry have been reported. These tetraphenylmethane derivatives are decorated at the periphery with a large panel of groups or functions, which include for instance halogens,[27] pyridine rings,[28] triazine derivatives,[29] boronic acids,[30] silanols,[31] amide connections,[32] cyano functions,[33] oligophenyl groups,[34] carboxylic acids,[35] sulfonic acids,[36] nitro groups[37] and acetylenic derivatives.[38] However, for the tetraphenylmethane-based building block containing phenol functionalities only one example of a molecule that self-assembles into a zeolitic network without the need of a co-crystal agent has been reported.[39] Thus, in the aim to characterise novel clathrate structures based on tetraphenylmethane derivatives, the *ortho*-methoxy-substituted tetraphenylmethane derivative (**6′**) crystallises in the space group *Pbcn* as an inclusion compound. However, due to the presence in the structure of highly disordered solvent molecules, which could not be refined satisfactorily, the SQUEEZE command was used to resolve the structure. The molecular structure is shown in Fig. 13, the crystallisation of (**6**) and (**6′**) was undertaken. Single crystals of (**6′**) suitable for X-ray analysis were obtained when toluene was allowed to slowly diffuse in a dichloromethane solution of (**6′**).

This structure indicates that in the crystal (**6′**) adopts a C_2 symmetry, since the two 1,3-dimethoxybenzene groups that decorate the tetraphenylmethane core adopt an *anti–anti* conformation whereas the two other groups display a *syn–anti* conformation. As shown in Fig. 13c, the crystalline network of (**6′**) leads to a zeolite-like structure, where the 1D-channels are originated from the association of four molecules *via* weak interactions (Fig. 13b). Such a tetrameric motif is essentially

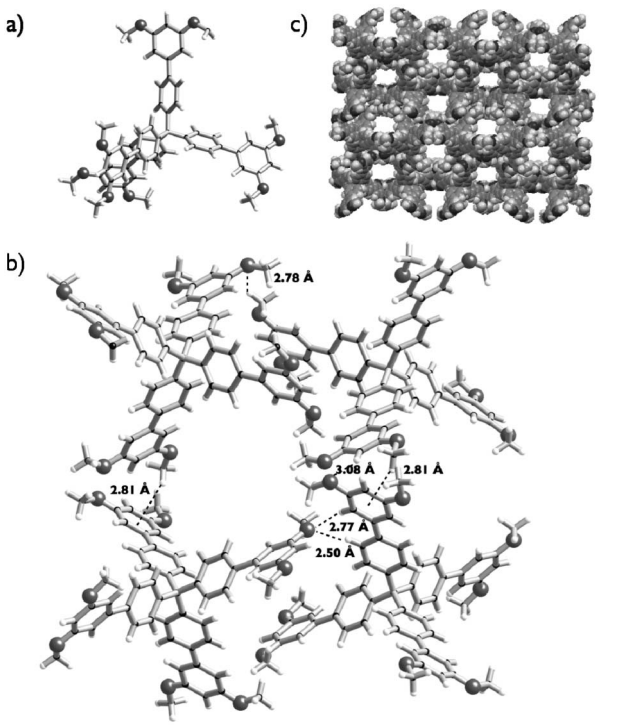

Fig. 13 The molecular structure of (**6′**) is shown in (a). A view along the *y*-axis of a tetrameric motif that permits the formation of 1D-channels is shown in (b). The tetrameric assembly formation is induced by several weak interactions. Different types of short contacts are identified as represented on the figure by dotted lines (the distances indicated here correspond to the hydrogen–oxygen distances or the hydrogen-centroid phenyl ring distances estimated from the structure. A space filling representation of the zeolite-like structure of (**6′**) self-assembled network is shown in (c), viewed along the *y*-axis.

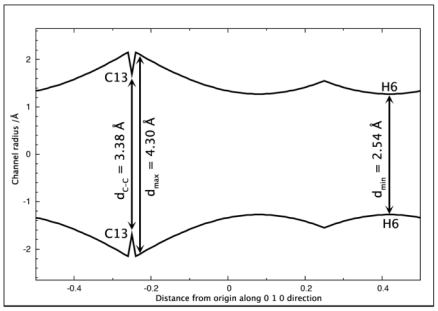

Fig. 14 Channel aperture along the [010] axis assuming van der Waals radii of 1.2, 1.52 and 1.7 Å for H, O and C-atoms in the crystal of (**6′**).

generated by CH···π, CH···O interactions as well as π–π interactions, as attested by the short contact distances measured from the structure (see Fig. 13b).

Interestingly, the inner diameter of the channel is ranging from 4.9 Å and 3.9 Å, as demonstrated in the channel aperture profile shown in Fig. 14. The solvent-accessible free volume of these channels is estimated to represent 20.9% of the total crystal volume.[40] Next, to better characterise this organic crystalline materials, the synthesis of a crystalline powder using the same solvent conditions as those employed to produce the single crystals was attempted.

Upon scale-up of the quantity of (**6′**) for crystallisation, the resulting crystalline powder was shown to be a second polymorph of (**6′**), since the X-ray diffraction powder pattern of the as-synthetized powder is strongly different from the one simulated from the X-ray single crystal diffraction data. The thermogravimetric analysis (TGA) performed on the crystalline powder evidenced no significant weight loss indicating the presence of an apohost phase. From its MVDP the (**6′**)-molecule has a Rsd radius of 6.81 Å for a volume of 1323 Å^3. The complete van der Waals topology corresponds to a new original uninodal 20-connected net having the point symbol $\{3^{54}.4^{126}.5^{10}\}$. Molecule (**6′**) was found to be rather polar (μ = 1.70 D), leading to a quite large packing energy: PE = −57 kJ mol^{-1}. Each (**6′**)-molecule being in contact with twenty other (**6′**)-molecules, the average interaction energy per contact is $<E_{int}>$ = −57/20 = −2.9 kJ mol^{-1}, a value much too high for pure van der Waals bonding. Generating a (**6′**)-chain allows us to derive an interaction energy E_{chain}(**6′**···**6′**) = −18 kJ mol^{-1}, corresponding clearly to π–π interactions. Linking chains into 2D-layers then leads to E_{int}(chain···chain) = −9 kJ mol^{-1}, and finally stacking layers together gives E_{int}(layer···layer) = −30 kJ mol^{-1}.

Single crystals of the T_d symmetric derivative (**6**) display the space group *C*2/*c* and were grown in an ethylacetate solution upon slow diffusion of toluene. The structure was solved using the Squeeze command due to the presence to highly disordered solvent molecules within the structure. The structure analysis also revealed that the solid-state organisation of (**6**) led to a network with 1D channels (Fig. 15). A close observation of the structure indicates that the 1D channels are generated by the assembly of infinite columns. These columns result from the stack of 6 units *via* CH···O interactions. Perpendicularly to these columns, the recognition between one 6 molecule with eight neighbouring molecules is originated from a complex hydrogen-bond dominated pattern, implying four resorcinol units as highlighted by the expansion shown in Fig. 15b. The simulation of the channel profile indicates the lake of homogeneity concerning the inner diameter of the channel where the inner diameter of the channel is ranging from 4.3 Å to 2.54 Å (Fig. 16). A guest accessible volume of approximately 28% of the volume of the crystal[40] has been estimated that is in the same accessible volume range as the one already reported for tetrakis(4-hydroxyphenyl)methane.[39]

Molecules of (**6**) have a Rsd radius of 6.53 Å for a volume of 1165 Å^3. The topology of the complete van der Waals net of the crystal was found to be a uninodal 14-connected net having the point symbol $\{3^{36}.4^{46}.5^{9}\}$, with fourteen contacts with other (**6**)-molecules corresponding to the known **gpu-x** topology in the RCSR database. Considering only H-bonding interactions between molecular tectons, the topological type was found to be that of a **sql**/Shubnikov tetragonal plane net having a point symbol $\{4^4.6^2\}$. In order to check if this molecule was indeed able to build a 3D-net, the atomic positions of the four H-atoms bonded to oxygen atoms O1–O4 were optimized through minimization of the PACHA lattice energy leading to a **bcu**-topology corresponding to a uninodal 8-connected net having a point symbol $\{4^{24}.6^4\}$. The molecular dipolar moment of (**6**) was found to be μ = 0.31 D with an overall packing energy PE = −134 kJ mol^{-1}.

Ten supramolecular interactions may be identified in this net: two bifurcated H-bonds (O3–H3···O2 = 206 pm and O3–H3···O4 = 235 pm), two non-bifurcated H-bonds (O1–H1···O3 = 183 pm) and four O–H···π bonds (O2–H2···Ph = 244 pm and O4–H4···Ph = 266 pm). In order to quantify the relative magnitude of each of these contributions, full rotation of the four O–H moieties along their respective C–O were performed in order to retrieve the respective energy profiles (Fig. 17).

The largest stabilizing energy (−57 kJ mol^{-1}) is lost after breaking the O3–H3 bifurcated H-bond (bottom left of Fig. 17). Then comes the O2–H2 π-interaction (top right with −48 kJ mol^{-1}) and the O1–H1 single H-bond (top left with −41 kJ mol^{-1}). Finally, the least stabilizing energy is associated to the O4–H4 π-interaction (bottom right with −21 kJ mol^{-1}).

By employing the same crystallisation conditions as the ones described just above, we were able to produce on a preparative scale crystals of (**6**) with a very high degree of reproducibility. The obtained phase was identical to the one evaluated by the single crystal analysis as confirmed by X-ray powder analysis. The capacity to produce crystals on a large scale allowed us to study more in detail the thermal behaviour of this porous network. The presence of guests trapped into the channels was confirmed by thermogravimetric analysis (TGA). A weight loss of 18.5% between 30 °C and 250 °C was observed. For this range of temperature, a closer observation of the TGA curve indicates three inflection regions that are linked with three endotherms measured at 80 °C, 120 °C and 160 °C by DSC. Obviously, these endothermic processes correspond to the desolvation of the crystallisation solvents (ethyl acetate, bp = 77 °C and toluene bp = 110 °C). Whereas the two first endotherms may be attributed to free molecules,

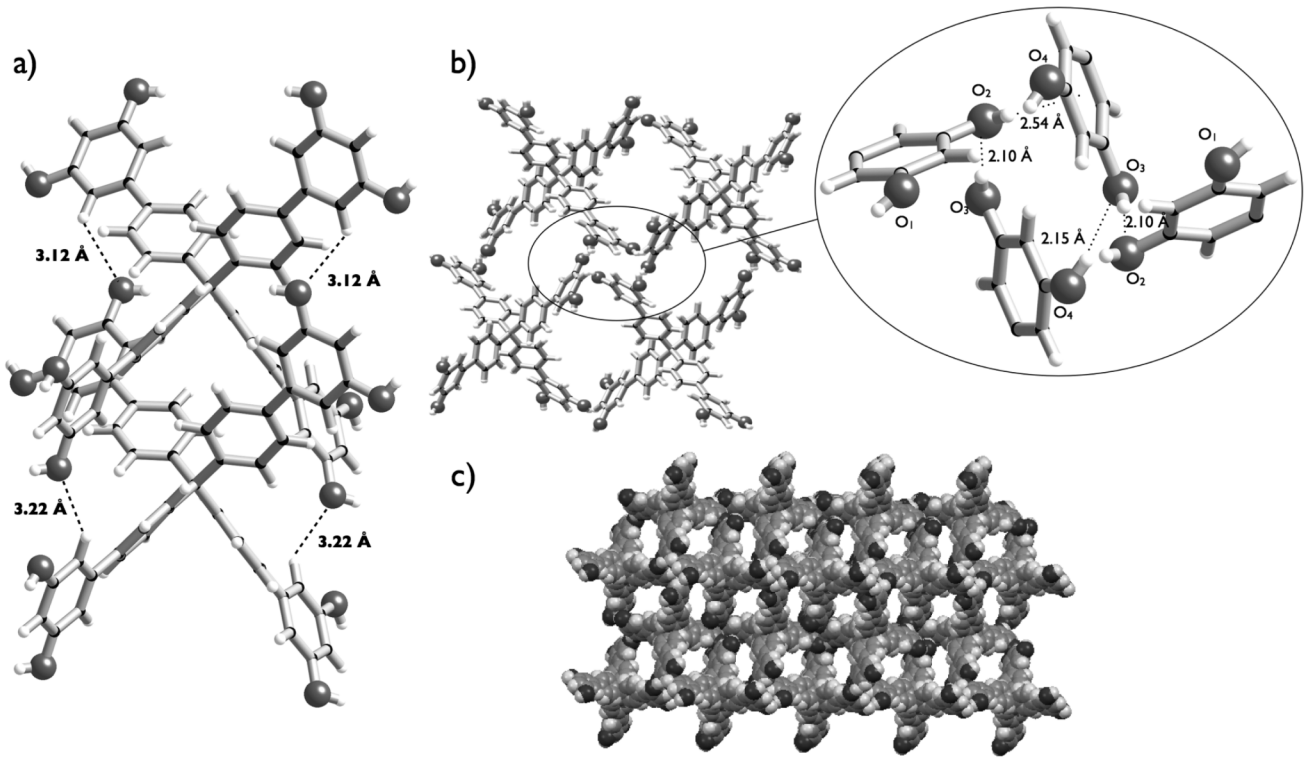

Fig. 15 A view along the *z*-axis of two stacked (**6**) molecules through CH···O interactions (mean intermolecular H···O distance: 3.17 Å) is shown in (a). The repetition of this motif leads to two infinite columnar assemblies. A view along the *y*-axis of four columnar assemblies is shown in (b). The interactions between a molecule of (**6**) with the neighbouring partners that belong to other columns are mainly due to hydrogen bonds. The expansion shows the complex recognition motif between four resorcinol units that belong respectively to four different (**6**) molecules. A space filling representation of the zeolite-like structure of the (**6**) self-assembled network is shown in (c), viewed along the *y*-axis.

the last endotherm is unambiguously linked to the departure of solvent molecules that are trapped into the channels. Thus, to evaluate the possibility to obtain a crystalline apohost phase *via* a thermal treatment, the X-ray diffraction powder analysis at various temperatures was performed from 30 °C to 190 °C. Fig. 18 shows three selected X-ray powder diffractograms. First of all, no phase transformation was observed upon elevating the temperature of the crystalline sample. Obviously, the temperature induces a dramatic loss of crystallinity. However, when the X-ray diffractogram was recorded at 130 °C, (*i.e.* after the two first desolvation processes according the DSC analysis), the solid conserves a certain degree of crystallinity but when all the solvent is removed from the structure (at 170 °C) the resulting apohost phase is amorphous. Nevertheless, at this stage the preservation of porosity for the apohost phase could not be excluded.

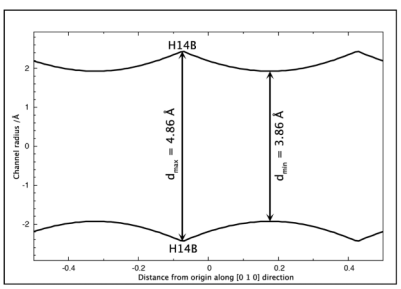

Fig. 16 Channel aperture along the [010] axis assuming van der Waals radii of 1.2; 1.52 and 1.7 Å for H, O and C-atoms in the crystal of (**6**).

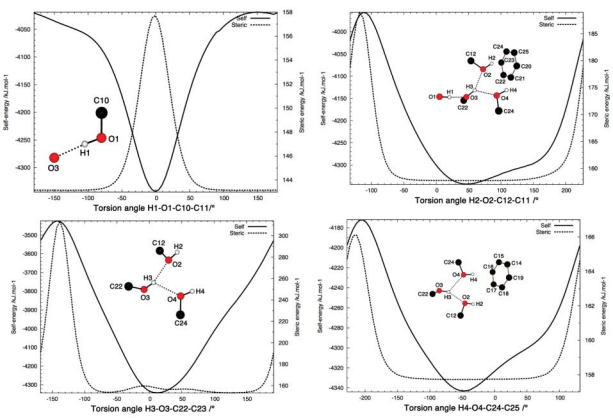

Fig. 17 Energy profiles for the 4 kinds of supramolecular interactions at work in the **bcu** net (Z = 4) based on (**6**). The full lines show the variation of the total electrostatic polarisation energy (self) when a given O–H moiety is rotated along its C–O bond by 360°. The dotted lines show the variation of the total electron–electron repulsions (steric) computed using Gordon–Kim potentials.

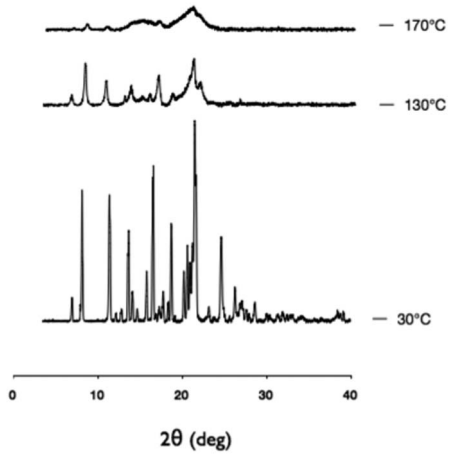

Fig. 18 Three X-ray powder diffractograms of the (**6**) crystalline powder recorded at 30 °C, 130 °C and 170 °C.

Conclusions

In conclusion, we have been able to synthesise and characterise several new resorcinol-based oligophenylene molecules displaying highly symmetric structures and that were able to self-assemble into interesting topologies through van der Waals and/or aromatic π–π stacking for methoxy-protected compounds and through H-bonding interactions in the case of deprotected molecules.

Concerning the methoxy-protected compounds, uninodal nets displaying connectivities ranging from 14 to 20 have been observed, with the exception of (**1′**), which forms a binodal 15-connected net. Most interestingly, most of the observed topologies are unprecedented with the exception of (**2′**) and (**3′**) that adopt the familiar **bct**-topology. Obviously, the highest connectivity was observed with (**6′**) that has 8 aromatic rings and the lowest one for (**2′**) that has only 3 aromatic rings. But it is worth noticing that (**4′**), which has also 3 aromatic rings, forms an 18-connected net whereas (**1′**) with only 2 rings forms a 15-connected net. Similarly it was observed that (**3′**) leads to a 14-connected net like (**2′**), whereas (**5′**) leads to a 19-connected net despite the fact that both molecules have the same number of aromatic rings. The number of aromatic rings is thus not a good discriminator for predicting the net connectivity and explaining the trends observed for melting points. However, dividing the packing energy by the net connectivity leads to the following order: −1.3 (**4′**) > −1.4 (**2′**), (**3′**) > −1.8 (**1′**) > −2.4 (**5′**) > −2.9 (**6′**) and this could nicely explain the rather low melting point of (**4′**) and quite high melting point of (**6′**) relative to the other members of the series. Obviously, a perfect correlation would not be expected owing to the fact that upon melting both enthalpy (packing energies) and entropy (degrees of freedom) factors have to be taken into account. Finally, only (**1′**), (**5′**) and (**6′**) were found to be associated through aromatic π–π stacking with interaction energies ranging from −14 kJ mol^{-1} down to −18 kJ mol^{-1}.

Replacing the methoxy groups by hydroxy groups allowed the occurrence of hydrogen bonding interactions with H-bond energies ranging from −17 kJ mol^{-1} down to −57 kJ mol^{-1}. The weakest bonds involved intermolecular H-bonds between phenolic groups whereas the strongest bonds involved intermolecular H-bonds with small solvent molecules such as water, ethylacetate or acetone. It is worth noticing that in all cases it was not possible to obtain molecular nets free of solvent molecules. When it was possible to localise solvent molecules, in the cases of (**1**), (**2**) and (**5**), quite complex unprecedented topologies have been evidenced, with connectivities ranging from 18-c up to 28-c taking into account both van der Waals and H-bonding and connectivities of 8-c or 9-c considering H-bonding alone. Compound (**6**) was a special case as, owing to its largely porous structure, it was not possible to localise solvent molecules. This explains the low value (14-c) found for the van der Waals plus H-bonding connectivity. The occurrence of quite strong aromatic O–H···π bonding interactions in addition to normal O–H···O bonding and the occurrence of a bifurcated H-bond are also worth noticing in this last case. Our inability to obtain single-crystals for compounds (**3**) and (**4**) could well be due to an obviously more flexible character for (**3**) and to a rather low symmetry for (**4**) favouring strong solvation in solution. The next step is now to investigate how these molecules may react with Ti(IV) tetraalkoxides in order to obtain Ti–O based MOFs absorbing visible rather than ultra-violet light. Work is under progress and results will be reported elsewhere.

Experimental section

General

All chemicals, solvents and reagents were of the best commercially available grade and purchased from Alfa Aesar, Sigma Aldrich, TCI Europe or Fluka and used as received. All reactions involving moisture-sensitive reactants were conducted under a nitrogen atmosphere. Column chromatography was performed on silica gel 60 (particle size: 40–63 μm, Merck, Darmstadt, Germany). For thin-layer chromatography silica gel 60 sheets (POLYGRAM SIL G/UV_{254}, Macherey-Nagel, Düren, Germany) were used, detected under UV-light at 254 nm. ^{1}H and ^{13}C NMR spectra were recorded with a Bruker Avance 300 (300 MHz) spectrometer with use of a deuterated solvent as the lock. The chemical shifts were expressed in parts per million (ppm, δ) and referenced to residual solvent protons as internal standards (^{1}H NMR: $CDCl_3$: δ = 7.26 ppm, CD_3OD: δ = 3.31 ppm; ^{13}C NMR: $CDCl_3$: δ = 77.16 ppm, CD_2Cl_2: δ = 53.84 ppm, CD_3OD: δ = 49.00 ppm). All coupling constants are absolute values and J values are expressed in Hertz (Hz). The description of signals include: s singlet, d doublet, dd doublet of doublets, t triplet, m multiplet. The signal abbreviations include: PhH aromatic proton, OMe methoxy proton. Infrared (IR) spectra were recorded with a Shimadzu FTIR-8400S. Fluorescence spectra were recorded with a Perkin Elmer LS55 Fluorescence Spectrometer. UV-vis spectra were recorded with a BioTek UVIKON XL spectrometer. Thermogravimetric

analysis (TGA) were performed on a Perkin Elmer Pyris 6 TGA thermogravimetric analyzer. Differential Scanning Calorimetry (DSC) spectra were obtained with a Perkin Elmer Jade DSC calorimeter. Melting points (M.p.) were determinated using a Stuart Scientific Melting Point SMP1 apparatus. Mass spectra were obtained with a micrOTOF in positive mode (ESI-MS). Microanalyses were performed by the Service de Microanalyses de la Fédération de Recherche de Chimie, Université de Strasbourg, Strasbourg, France. Crystallography data were collected at 173(2) K with a Bruker APEX8 CCD diffractometer equipped with an Oxford cryosystem liquid N_2 device, with use of graphite-monochromated Mo Kα (λ = 0.71073) radiation. For all structures, diffraction data were corrected for absorption, and structural determination was achieved by using the APEX (1.022) package. Tetrakis(4-bromophenyl)methane was obtained according ref. 41.

3,3′,5,5′-Tetramethoxy-1,1′-biphenyl (1′)[18]

To a stirred solution of 3,5-dimethoxybenzeneboronic acid (170 mg, 0.93 mmol) in methanol (19 mL) was added $Pd(OAc)_2$ (20.9 mg, 0.09 mmol). The mixture was stirred under air for five hours at room temperature and concentrated under reduced pressure. The remaining crude product was purified by silica gel chromatography (CH_2Cl_2/*n*-pentane, 50/50) to yield a white solid (127 mg, 98%). M.p. 108 °C (lit. 109–111 °C). ^{1}H NMR (300 MHz, $CDCl_3$): δ = 6.69 (d, J = 2.2 Hz, 4H, PhH), 6.45 (t, J = 2.2 Hz, 2H, PhH), 3.82 (s, 12H, OMe) ppm. ^{13}C NMR (75 MHz, $CDCl_3$): δ = 161.5, 143.7, 105.8, 99.8, 55.8 ppm. IR: $\tilde{\nu}$ = 3006, 1604, 1577, 1470, 1410, 1291, 1195, 1156, 1030, 861, 845, 816, 692 cm^{-1}. Crystals were obtained by slow diffusion of *n*-pentane into a CH_2Cl_2 solution of **1**. X-ray data for **1**: empirical formula: $C_{16}H_{18}O_4$; formula mass: 274.30; crystal system: orthorhombic; space group: $Pna2_1$; unit cell dimensions: a = 16.655(3) Å, b = 7.4707(7) Å, c = 22.232(3) Å; V = 2766.3(6) Å^3; Z = 8; density (calcd): 1.317 Mg m^{-3}; crystal size: 0.12 × 0.09 × 0.01 mm; θ range for data collection: 1.83–27.53°; reflections collected: 8997; independent reflections: 4044 [R_{int} = 0.0283]; refinement method: full-matrix least squares on F^2; data/restraints/parameters: 4044/1/370; goodness-of-fit on F^2: 1.001; final R indices [$I > 2\sigma(I)$]: R_1 = 0.0417, wR_2 = 0.0934; R indices (all data): R_1 = 0.0508, wR_2 = 0.1005. CCDC: 934379.

3,3′,5,5′-Tetrahydroxy-1,1′-biphenyl (1)[18]

The reaction was conducted under nitrogen. At −78 °C, to a solution of **1** (1 g, 3.65 mmol) in freshly distilled CH_2Cl_2 (20 mL) was added dropwise a solution of BBr_3 (1 M in CH_2Cl_2, 17.5 mL). The resulting reaction mixture was allowed to reach room temperature and stirred overnight. Then, a small amount of water was carefully added (40 mL). The mixture was washed with an aqueous Na_2CO_3 solution (2 M, 200 mL) and then acidified with HCl 37% until acid pH was reached. The water phase was extracted three times with diethyl ether and the organic layers were combined and concentrated under reduced pressure to afford **1** as a brownish powder (795 mg, quantitative). M.p. > 300 °C (lit. 310 °C). ^{1}H NMR (300 MHz, CD_3OD): δ = 6.46 (d, J = 2.2 Hz, 4H, PhH), 6.22 (t, J = 2.2 Hz, 2H, PhH) ppm. ^{13}C (75 MHz, CD_3OD): δ = 158.8, 142.7, 108.4, 102.5 ppm. IR: $\tilde{\nu}$ = 3282, 2968, 1618, 1424, 1292, 1153, 1136, 1002, 817, 748, 672 cm^{-1}. Crystals were obtained by slow evaporation of a solution of **1** in ethanol. X-ray data for **1**: empirical formula: $C_{12}H_{14}O_6$ ($C_{12}H_{10}O_4$, $2H_2O$); formula mass: 254.23; crystal system: triclinic; space group: $P\bar{1}$; unit cell dimensions: a = 4.9700(2) Å, b = 7.4370(3) Å, c = 7.9748(4) Å; α = 85.355(2), β = 82.615(2), γ = 75.241(2); V = 282.32(2) Å^3; Z = 1; density (calcd): 1.495 Mg m^{-3}; crystal size: 0.09 × 0.07 × 0.05 mm; θ range for data collection: 2.58–27.00°; reflections collected: 2867; independent reflections: 1205 [R_{int} = 0.0160]; refinement method: full-matrix least squares on F^2; data/restraints/parameters: 1205/3/90; goodness-of-fit on F^2: 1.060; final R indices [$I > 2\sigma(I)$]: R_1 = 0.0454, wR_2 = 0.1330; R indices (all data): R_1 = 0.0511, wR_2 = 0.1396. CCDC: 934386.

3,3′′,5,5′′-Tetramethoxy-1,1′:4′,1′′-terphenyl (2′)

The reaction was conducted under a nitrogen atmosphere. A degassed aqueous solution of Na_2CO_3 (2 M, 40 mL) was transferred by cannula to a degassed solution of 1,4-dibromobenzene (500 mg, 2.12 mmol) and $Pd(PPh_3)_4$ (120 mg) in toluene (40 mL). After the cannulation of a solution of 3,5-dimethoxy-phenylboronic acid (1.07 g, 5.88 mmol) in MeOH (40 mL), the reaction mixture was refluxed overnight. The mixture was allowed to reach room temperature and extracted three times with CH_2Cl_2. The combined organic layers were dried over $MgSO_4$ and concentrated under reduced pressure. The crude product was purified over a silica gel chromatography (CH_2Cl_2/*n*-pentane 50/50) to give **2′** as a white powder (606 mg, 82%). M.p. 149–150 °C. ^{1}H NMR (300 MHz, $CDCl_3$): δ = 7.63 (s, 4H, PhH), 6.76 (d, J = 2.1 Hz, 4H, PhH), 6.47 (t, J = 2.1 Hz, 2H, PhH), 3.85 (s, 12H, OMe) ppm. ^{13}C NMR (75 MHz, $CDCl_3$): δ = 161.5, 143.1, 140.7, 127.8, 105.6, 99.7, 55.8 ppm. IR: $\tilde{\nu}$ = 2947, 2836, 1608, 1583, 1462, 1332, 1228, 1201, 1162, 1037, 1014, 940, 826, 689 cm^{-1}. MS (ESI): calcd for $[M + Na]^+$ 373.142, found 373.141. $C_{22}H_{22}O_4$ (350.15): calcd C 75.41, H 6.33; found C 74.31, H 6.32%. Crystals were obtained by slow diffusion of *n*-pentane into a CH_2Cl_2 solution of **2′**. X-ray data for **2′**: empirical formula: $C_{22}H_{22}O_4$; formula mass: 350.40; crystal system: monoclinic; space group: $P2_1/c$; unit cell dimensions: a = 13.0066(5) Å, b = 8.3251(3) Å, c = 8.5054(3) Å; β = 106.143(2)°; V = 884.66(6) Å^3; Z = 2; density (calcd): 1.315 Mg m^{-3}; crystal size: 0.10 × 0.07 × 0.06 mm; θ range for data collection: 1.63–29.99°; reflections collected: 21 371; independent reflections: 2550 [R_{int} = 0.0253]; refinement method: full-matrix least squares on F^2; data/restraints/parameters: 2550/0/120; goodness-of-fit on F^2: 1.078; final R indices [$I > 2\sigma(I)$]: R_1 = 0.0457, wR_2 = 0.1384; R indices (all data): R_1 = 0.0607, wR_2 = 0.1595. CCDC: 934380.

3,3′′,5,5′′-Tetrahydroxy-1,1′:4′,1′′-terphenyl (2)

The reaction was conducted under a nitrogen atmosphere. At −78 °C, to a solution of **2′** (475 mg, 1.36 mmol) in freshly distilled CH_2Cl_2 (10 mL) was added dropwise a solution of BBr_3 (1 M in CH_2Cl_2, 6.51 mL). The resulting reaction mixture was stirred overnight at room temperature. Then, a small amount of water was carefully added (10 mL). The mixture was washed with an aqueous Na_2CO_3 solution (2 M, 200 mL) and then acidified with HCl 37% until acid pH was reached. The solid was recovered by filtration and dried under reduced pressure to afford **2** as a brownish powder (370 mg, 93%). M.p.

> 300 °C. ^{1}H NMR (300 MHz, CD_3OD): δ = 7.57 (s, 4H, PhH), 6.57 (d, J = 2.2 Hz, 4H, PhH), 6.26 (t, J = 2.2 Hz, 2H, PhH). ^{13}C NMR (75 MHz, CD_3OD): δ = 160.1, 144.3, 141.7, 128.3, 106.7, 102.9 ppm. IR: $\tilde{\nu}$ = 3280, 1595, 1487, 1345, 1151, 1001, 867, 818, 678 cm^{-1}. MS (MALDI-TOF): calcd for $[M]^+$ 294.09, found 294.20. $C_{18}H_{14}O_4$ (294.09)·$2H_2O$: calcd C 65.45, H 5.49; found C 65.96, H 5.25%. Crystals were obtained by slow evaporation of a solution of **2** in ethyl acetate. X-ray data for **2** (the structure was solved using the SQUEEZE command): empirical formula: ($4C_{18}H_{14}O_4$, $C_4H_8O_2$, $6H_2O$); formula mass: 1479.49; crystal system: monoclinic; space group: $P2_1/c$; unit cell dimensions: a = 15.0657(3) Å, b = 9.2696(2) Å, c = 28.1087(6) Å; β = 91.7970(10)°; V = 3923.53(14) Å^3; Z = 2; density (calcd): 1.252 Mg m^{-3}; crystal size: 0.11 × 0.08 × 0.06 mm; θ range for data collection: 1.95–28.34°; reflections collected: 35 365; independent reflections: 9642 [R_{int} = 0.0564]; refinement method: full-matrix least squares on F^2; data/restraints/parameters: 9643/11/480; goodness-of-fit on F^2: 1.052; final R indices [$I > 2\sigma(I)$]: R_1 = 0.0820, wR_2 = 0.2526; R indices (all data): R_1 = 0.1189, wR_2 = 0.2763. CCDC: 934375.

3,3′′,5,5′′-Tetramethoxy-1,1′:3′,1′′-terphenyl (4′)

The reaction was conducted under a nitrogen atmosphere. A degassed aqueous solution of Na_2CO_3 (2 M, 64 mL) was transferred by cannula to a degassed solution of 1,3-dibromobenzene (1.89 g, 8 mmol) and $Pd(PPh_3)_4$ (0.45 g) in toluene (64 mL). After the cannulation of a solution of 3,5-dimethoxyphenylboronic acid (3.40 g, 18.7 mmol) in MeOH (62 mL), the reaction mixture was refluxed overnight. The mixture was allowed to reach room temperature and extracted three times with CH_2Cl_2. The combined organic layers were dried over $MgSO_4$ and concentrated under reduced pressure. The crude product was purified over a silica gel chromatography (CH_2Cl_2/*n*-pentane 50/50) to give **4′** as a white powder (2.47 g, 88%). M.p. 87 °C. ^{1}H NMR (300 MHz, $CDCl_3$): δ = 7.77 (t, J = 1.8 Hz, 1H, PhH), 7.58 (t, J = 1.8 Hz, 1H, PhH), 7.51 (m, 2H, PhH), 6.78 (d, J = 2.2 Hz, 4H, PhH), 6.49 (t, J = 2.2 Hz, 2H, PhH), 3.86 (s, 12H, PhH) ppm. ^{13}C NMR (75 MHz, $CDCl_3$): δ = 161.1, 143.4, 141.8, 129.1, 126.5, 126.2, 105.6, 99.5, 55.5 ppm. IR: $\tilde{\nu}$ = 3000, 1591, 1461, 1421, 1388, 1345, 1295, 1295, 1201, 1154, 1065, 923, 842, 824, 794, 697 cm^{-1}. MS (ESI) calcd for $[M + Na]^+$ 373.14, found 373.14. $C_{22}H_{22}O_4$: calcd C 75.41, H 6.33; found C 75.37, H 6.37%. Crystals were obtained by slow diffusion of *n*-pentane into a CH_2Cl_2 solution of **5**. X-ray data for **4′**: empirical formula: $C_{22}H_{22}O_4$; formula mass: 350.40; crystal system: triclinic; space group: $P\bar{1}$; unit cell dimensions: a = 7.8893(2) Å, b = 9.9296(2) Å, c = 11.9272(3) Å; α = 74.7250(10)°, β = 81.3570(10)°, γ = 83.1840(10)°; V = 888.04(4) Å^3; Z = 2; density (calcd): 1.310 Mg m^{-3}; crystal size: 0.12 × 0.10 × 0.10 mm; θ range for data collection: 1.78–30.11°; reflections collected: 12 010; independent reflections: 4728 [R_{int} = 0.0184]; refinement method: full-matrix least squares on F^2; data/restraints/parameters: 4728/0/239; goodness-of-fit on F^2: 1.035; final R indices [$I > 2\sigma(I)$]: R_1 = 0.0424, wR_2 = 0.1159; R indices (all data): R_1 = 0.0538, wR_2 = 0.1246. CCDC: 934377.

[1,1′:3′,1′′-Terphenyl]-3,3′′,5,5′′-tetraol (4)

The reaction was conducted under nitrogen. At −78 °C, to a solution of **4′** (0.670 g, 1.9 mmol) in freshly distilled CH_2Cl_2 (10 mL) was added dropwise a solution of BBr_3 (1 M in CH_2Cl_2, 9.2 mL). The resulting reaction mixture was allowed to reach room temperature and stirred overnight. Then, a small amount of water was carefully added (10 mL). The mixture was washed with an aqueous Na_2CO_3 solution (2 M, 20 mL) and then acidified with HCl 37% until acid pH was reached. The precipitate formed was filtered, washed with an excess of water and dried under reduced pressure to afford **4** as a white solid (560 mg, quantitative). M.p. > 300 °C. ^{1}H NMR (300 MHz, CD_3OD): δ = 7.67 (t, J = 1.7 Hz, 1H, PhH), 7.48 (t, J = 2 Hz, 1H, PhH), 7.43 (m, 2H, PhH), 6.57 (d, J = 2 Hz, 4H, PhH), 6.27 (t, J = 2.2 Hz, 2H, PhH) ppm. ^{13}C NMR (75 MHz, CD_3OD): δ = 159.9, 144.5, 143.0, 129.9, 126.8, 126.3, 106.6, 102.6 ppm. IR: $\tilde{\nu}$ = 3340, 3180, 1606, 1597, 1511, 1472, 1332, 1306, 1210, 1155, 1007, 824, 773, 708, 677 cm^{-1}. MS (ESI) calcd for $[M + Na]^+$ 317.08, found 317.08. $C_{18}H_{14}O_4$ (294.09)·$2H_2O$: calcd C 65.45, H 5.49; found C 64.97, H 5.56%.

3,3′′′,5,5′′′-Tetramethoxy-1,1′:4′,1′′:4′′,1′′′-quaterphenyl (3′)

The reaction was conducted under a nitrogen atmosphere. A degassed aqueous solution of Na_2CO_3 (2 M, 60 mL) was transferred by cannula to a degassed solution of 1-bromo-3,5-dimethoxybenzene (1.375 g, 6.33 mmol) and $Pd(PPh_3)_4$ (0.120 g) in toluene (60 mL). After the cannulation of a solution of biphenyl-4,4′-diboronic acid bis(neopentyl glycol) ester (1 g, 2.64 mmol) in MeOH (60 mL), the reaction mixture was refluxed during four days. The mixture was allowed to reach room temperature and extracted three times with CH_2Cl_2. The combined organic layers were dried over $MgSO_4$ and concentrated under reduced pressure. The crude product was purified over a silica gel chromatography (CH_2Cl_2/*n*-pentane 50/50) to give **3′** as a white powder (1.012 g, 90%). M.p. 162–163 °C. ^{1}H NMR (300 MHz, $CDCl_3$): δ = 7.72 (dd, J = 8.8 Hz, J = 4.6 Hz, 8H, PhH), 6.81 (d, J = 2.3 Hz, 4H, PhH), 6.49 (t, J = 2.3 Hz, 2H, PhH), 3.86 (s, 12H, OMe) ppm. ^{13}C NMR (75 MHz, $CDCl_3$): δ = 161.7, 143.1, 140.5, 140.1, 127.9, 127.6, 105.6, 99.8, 55.8 ppm. IR: $\tilde{\nu}$ = 3002, 2945, 2833, 1586, 1460, 1332, 1220, 1202, 1163, 1082, 1040, 1030, 821, 688 cm^{-1}. MS (ESI) calcd for $[M + H]^+$ 427.191, found 427.181. $C_{28}H_{26}O_4$ (426.18): calcd C 78.85, H 6.14; found C 76.42, H 6.30%. Crystals were obtained by slow diffusion of *n*-pentane into a CH_2Cl_2 solution of **3′**. X-ray data for **3′**: empirical formula: $C_{28}H_{26}O_4$; formula mass: 426.49; crystal system: monoclinic; space group: $P2_1/c$; unit cell dimensions: a = 15.6242(12) Å, b = 8.1550(6) Å, c = 8.4742(6) Å; β = 96.557(2)°, V = 1072.68(14) Å^3; Z = 2; density (calcd): 1.320 Mg m^{-3}; crystal size: 0.09 × 0.06 × 0.04 mm; θ range for data collection: 2.62–28.28°; reflections collected: 6060; independent reflections: 2637 [R_{int} = 0.0252]; refinement method: full-matrix least squares on F^2; data/restraints/parameters: 2637/0/147; goodness-of-fit on F^2: 1.045; final R indices [$I > 2\sigma(I)$]: R_1 = 0.0517, wR_2 = 0.1320; R indices (all data): R_1 = 0.0857, wR_2 = 0.1517. CCDC: 934387.

3,3′′′,5,5′′′-Tetrahydroxy-1,1′:4′,1′′:4′′,1′′′-quaterphenyl (3)

The reaction was conducted under a nitrogen atmosphere. At −78 °C, to a solution of **7** (700 mg, 1.64 mmol) in freshly distilled CH_2Cl_2 (45 mL) was added dropwise a solution of BBr_3 (1 M in CH_2Cl_2, 7.88 mL). The resulting reaction mixture was stirred overnight at room temperature. Then, a small

amount of water was carefully added (10 mL). The mixture was washed with an aqueous Na_2CO_3 solution (2 M, 400 mL) and then acidified with HCl 37% until acid pH. The water phase was extracted three times with diethyl ether and the organic layers were combined and concentrated under reduced pressure to afford **3** as a brownish powder (580 mg, 95%). M.p. > 300 °C. ^{1}H NMR (300 MHz, CD_3OD): δ = 7.70 (complex, 8H, PhH), 6.60 (d, J = 2.1 Hz, 4H PhH), 6.27 (t, J = 2.1 Hz, 2H, PhH) ppm. ^{13}C NMR (75 MHz, CD_3OD): δ 102.5, 108.4, 127.2, 139.7, 142.7, 158.8 ppm. IR: $\tilde{\nu}$ = 3260, 2914, 2830, 1592, 1481, 1344, 1168, 1151, 998, 812, 681 cm^{-1}. MS (MALDI-TOF) calcd for $[M]^+$ 370.121, found 370.2.

5′-(3,5-Dimethoxyphenyl)-3,3′′,5,5′′-tetramethoxy-1,1′:3′,1′′-terphenyl (5′)

The reaction was conducted under a nitrogen atmosphere. A degassed aqueous solution of Na_2CO_3 (2 M, 64 mL) was transferred by cannula to a degassed solution of 1,3,5-tribromobenzene (1 g, 3.17 mmol) and $Pd(PPh_3)_4$ (0.18 g) in toluene (64 mL). After the cannulation of a solution of 3,5-dimethoxyphenylboronic acid (2.07 g, 11.4 mmol) in MeOH (62 mL), the reaction mixture was refluxed overnight. The mixture was allowed to reach room temperature and extracted three times with CH_2Cl_2. The combined organic layers were dried over $MgSO_4$ and concentrated under reduced pressure. The crude product was purified over a silica gel chromatography (CH_2Cl_2/*n*-pentane 50/50) to give **5′** as a white powder (1.387 g, 90%). M.p. 204 °C. ^{1}H NMR (300 MHz, $CDCl_3$): δ = 7.78 (s, 3H, PhH), 6.84 (d, J = 2.4 Hz, 6H, PhH), 6.51 (t, J = 2.2 Hz, 3H, PhH), 3.86 (s, 18H, OMe) ppm. ^{13}C NMR (75 MHz, $CDCl_3$): δ = 159.6, 141.5, 140.6, 123.8, 103.9, 97.9, 53.9 ppm. IR: $\tilde{\theta}$ = 3000, 2940, 1588, 1463, 1424, 1399, 1325, 1258, 1194, 1150, 1060, 830, 698, 675 cm^{-1}. MS (ESI) calcd for $[M + H]^+$ 487.212, found 487.199. $C_{30}H_{30}O_6$ (486.20): calcd C 74.06, H 6.21; found C 73.44, H 6.24%. Crystals were obtained by slow diffusion of *n*-pentane into a CH_2Cl_2 solution of **5′**. X-ray data for **5′**: empirical formula: $C_{30}H_{30}O_6$; formula mass: 486.54; crystal system: triclinic; space group: $P\bar{1}$; unit cell dimensions: a = 10.6996(4) Å, b = 10.8140(4) Å, c = 11.0347(4) Å; α = 84.070(2)°, β = 89.396(2)°, γ = 87.954(2)°; V = 1269.10(8) Å^3; Z = 2; density (calcd): 1.273 Mg m^{-3}; crystal size: 0.09 × 0.06 × 0.05 mm; θ range for data collection: 1.89–28.00°; reflections collected: 22 207; independent reflections: 5896 [R_{int} = 0.0387]; refinement method: full-matrix least squares on F^2; data/restraints/parameters: 5896/0/331; goodness-of-fit on F^2: 1.053; final R indices [$I > 2\sigma(I)$]: R_1 = 0.0512, wR_2 = 0.1377; R indices (all data): R_1 = 0.0821, wR_2 = 0.1573. CCDC: 934381.

5′-(3,5-Dihydroxyphenyl)-3,3′′,5,5′′-tetrahydroxy-1,1′:3′,1′′-terphenyl (5)

The reaction was conducted under a nitrogen atmosphere. At −78 °C, to a solution of **5′** (1 g, 2.21 mmol) in freshly distilled CH_2Cl_2 (20 mL) was added dropwise a solution of BBr_3 (1 M in CH_2Cl_2, 14.8 mL). The resulting reaction mixture was stirred overnight at room temperature. Then, a small amount of water was carefully added (40 mL). The mixture was washed with an aqueous Na_2CO_3 solution (2 M, 250 mL) and then acidified with HCl 37% until acid pH was reached. The precipitate formed was filtered, washed with an excess of water and dried under reduced pressure to afford **5** as a grayish solid (826 mg, quantitative). M.p. > 300 °C. ^{1}H NMR (300 MHz, CD_3OD): δ = 7.62 (s, 3H, PhH), 6.61 (d, J = 2.2 Hz, 6H, PhH), 6.29 (t, J = 2.2 Hz, 3H, PhH) ppm. ^{13}C NMR (75 MHz, CD_3OD): δ = 160.2, 144.8, 144.7, 125.8, 106.9, 103.0 ppm. IR: $\tilde{\nu}$ = 3282, 1610, 1592, 1512, 1490, 1428, 1335, 1195, 1156, 1002, 825, 686 cm^{-1}. MS (ESI) calcd for $[M + H]^+$ 403.118, found 403.117. $C_{24}H_{18}O_6$ (402.11)·4H_2O: calcd C 60.76, H 5.52; found C 60.67, H 5.42%. Crystals were obtained by slow diffusion of chloroform into an acetone solution of **5**. X-ray data for **5**: empirical formula: $C_{30}H_{32}O_9$ ($C_{24}H_{18}O_6$, 2C_3H_6O, H_2O); formula mass: 536.56; crystal system: monoclinic; space group: $P2_1/c$; unit cell dimensions: a = 12.0986(4) Å, b = 20.2849(5) Å, c = 11.2091(3) Å; β = 98.4490(10)°, V = 2721.07(13) Å^3; Z = 4; density (calcd): 1.310 Mg m^{-3}; crystal size: 0.06 × 0.05 × 0.05 mm; θ range for data collection: 1.98–29.08°; reflections collected: 22 721; independent reflections: 6951 [R_{int} = 0.0335]; refinement method: full-matrix least squares on F^2; data/restraints/parameters: 6951/3/368; goodness-of-fit on F^2: 1.001; final R indices [$I > 2\sigma(I)$]: R_1 = 0.0472, wR_2 = 0.1236; R indices (all data): R_1 = 0.0753, wR_2 = 0.1403. CCDC: 934378.

Tetrakis(3′,5′-dimethoxy-[1,1′-biphenyl]-4-yl)methane (6′)

The reaction was conducted under a nitrogen atmosphere. A degassed aqueous solution of Na_2CO_3 (2 M, 60 mL) was transferred by cannula to a degassed solution of tetrakis(4-bromophenyl)methane (1.26 g, 1.98 mmol) and $Pd(PPh_3)_4$ (113 mg) in toluene (60 mL). After the cannulation of a solution of 3,5-dimethoxyphenylboronic acid (1.43 g, 7.92 mmol) in MeOH (60 mL), the reaction mixture was refluxed for 4 days. The mixture was allowed to reach room temperature and extracted three times with CH_2Cl_2. The combined organic layers were dried over $MgSO_4$ and concentrated under reduced pressure. The crude product was purified over a silica gel chromatography (CH_2Cl_2/*n*-pentane, 50/50) to give **6′** as a white solid (1.347 g, 80%). M.p. 270 °C. ^{1}H NMR (300 MHz, $CDCl_3$): δ = 7.55 (d, J = 8.4 Hz, 8H, PhH), 7.43 (d, J = 8.4 Hz, 8H, PhH), 6.75 (d, J = 2.2 Hz, 8H, PhH), 6.45 (t, J = 2.2 Hz, 4H, PhH) ppm. ^{13}C NMR (75 MHz, $CDCl_3$): δ = 161.6, 146.6, 143.0, 139.1, 131.7, 126.8, 105.5, 99.7, 64.7, 55.8 ppm. IR: $\tilde{\nu}$ = 2910, 1693, 1591, 1454, 1330, 1146, 1153, 1058, 1014, 814, 668 cm^{-1}. MS (ESI) calcd for $[M + Na]^+$ 887.355, found 887.334. $C_{57}H_{52}O_8$ (864.37): calcd C 79.14, H 6.06; found C 77.99, H 6.24%. Crystals were obtained by slow diffusion of toluene into a CH_2Cl_2 solution of **6′**. X-ray data for **6′**: empirical formula: $C_{57}H_{52}O_8$; formula mass: 864.99; crystal system: orthorhombic; space group: *Pbcn*; unit cell dimensions: a = 27.539(2) Å, b = 7.4754(4) Å, c = 25.6914(19) Å; V = 5289.0(6) Å^3; Z = 4; density (calcd): 1.086 Mg m^{-3}; crystal size: 0.06 × 0.05 × 0.02 mm; θ range for data collection: 1.48–28.36°; reflections collected: 38 147; independent reflections: 6409 [R_{int} = 0.1237]; refinement method: full-matrix least squares on F^2; data/restraints/parameters: 6409/0/299; goodness-of-fit on F^2: 1.002; final R indices [$I > 2\sigma(I)$]: R_1 = 0.0801, wR_2 = 0.1819; R indices (all data): R_1 = 0.1466, wR_2 = 0.2031. CCDC: 934382.

Tetrakis(3′,5′-dihydroxy-[1,1′-biphenyl]-4-yl)methane (6)

The reaction was conducted under a nitrogen atmosphere. At −78 °C, to a solution of **6′** (900 mg, 1.04 mmol) in freshly

distilled CH_2Cl_2 (60 mL) was added dropwise a solution of BBr_3 (1 M in CH_2Cl_2, 10 mL). The resulting reaction mixture was stirred two days at room temperature. Then, a small amount of water was carefully added (40 mL). The mixture was washed with an aqueous Na_2CO_3 solution (2 M, 100 mL) and then acidified with HCl 37% until acid pH was reached. The solid was recovered by filtration and dried under reduced pressure to afford **6** as a brownish powder (750 mg, 95%). M.p. > 300 °C. ^{1}H NMR (300 MHz, CD_3OD): δ = 7.47 (d, J = 8.4 Hz, 8H, PhH), 7.34 (d, J = 8.5 Hz, 8H, PhH), 6.56 (d, J = 2.2 Hz, 8H, PhH), 6.24 (t, J = 2.2 Hz, 4H, PhH) ppm. ^{13}C (75 MHz, CD_3OD): δ = 160.4, 147.7, 144.5, 140.8, 132.9, 127.5, 107.0, 103.1, 65.9 ppm. IR: $\tilde{\nu}$ = 3334, 1714, 1596, 1487, 1337, 1197, 1148, 998, 814, 669 cm^{-1}. MS (MALDI-TOF) calcd for $[M]^+$ 752.241, found 752.5. $C_{49}H_{36}O_8$ (752.24)·$5H_2O$: calcd C 69.82, H 5.50; C 69.29, H 4.98%. Crystals were obtained by slow diffusion of toluene into an ethyl acetate solution of **6**. X-ray data for **6**: empirical formula (the structure was solved using the SQUEEZE command): $C_{49}H_{36}O_8$; formula mass: 752.78; crystal system: monoclinic; space group: $C2/c$; unit cell dimensions: a = 32.8482(13) Å, b = 7.0555(2) Å, c = 25.7963(18) Å; β = 128.8150(10)°, V = 4658.3(4) Å^3; Z = 4; density (calcd): 1.073 Mg m^{-3}; crystal size: 0.07 × 0.05 × 0.05 mm; θ range for data collection: 1.59–28.29°; reflections collected: 21 732; independent reflections: 5685 [R_{int} = 0.0343]; refinement method: full-matrix least squares on F^2; data/restraints/parameters: 5685/0/262; goodness-of-fit on F^2: 1.052; final R indices [$I > 2\sigma(I)$]: R_1 = 0.0609, wR_2 = 0.1757; R indices (all data): R_1 = 0.0871, wR_2 = 0.1910. CCDC: 934376.

Acknowledgements

This work was performed at the Université de Strasbourg with public funds allocated by the Centre National de la Recherche Scientifique (CNRS) and the Ministère de l'Enseignement Supérieur et de la Recherche.

Notes and references

1 (*a*) J.-R. Li, Y. Ma, M. C. McCarthy, J. Sculley, J. Yu, H.-K. Jeong, P. B. Balbuena and H.-C. Zhou, *Coord. Chem. Rev.*, 2011, **255**, 1791; (*b*) J.-R. Li, R. J. Kuppler and H.-C. Zhou, *Chem. Soc. Rev.*, 2009, **38**, 1477; (*c*) K. Kim, M. Banerjee, M. Yoon and S. Das, *Top. Curr. Chem.*, 2010, **293**, 115; (*d*) E. D. Bloch, W. L. Queen, R. Krishna, J. M. Zadrozny, C. M. Brown and J. R. Long, *Science*, 2012, **335**, 1606; (*e*) S. Ma, D. Sun, X.-S. Wang and H.-C. Zhou, *Angew. Chem., Int. Ed.*, 2007, **46**, 2458–2462.

2 (*a*) L. J. Murray, M. Dincă and J. R. Long, *Chem. Soc. Rev.*, 2009, **38**, 1294; (*b*) A. U. Czaja, N. Trukhan and U. Müller, *Chem. Soc. Rev.*, 2009, **38**, 1284; (*c*) D. Yuan, D. Zhao, D. Sun and H.-C. Zhou, *Angew. Chem., Int. Ed.*, 2010, **49**, 5357; (*d*) S. Ma and H.-C. Zhou, *J. Am. Chem. Soc.*, 2006, **128**, 11734; (*e*) D. Sun, S. Ma, Y. Ke, D. J. Collins and H.-C. Zhou, *J. Am. Chem. Soc.*, 2006, **128**, 3896; (*f*) N. L. Rosi, J. Eckert, M. Eddaoudi, D. T. Vodak, J. Kim, M. O'Keeffe and O. M. Yaghi, *Science*, 2003, **300**, 1127.

3 (*a*) K. M. L. Taylor-Pashow, J. Della Rocca, Z. G. Xie, S. Tran and W. B. Lin, *J. Am. Chem. Soc.*, 2009, **131**, 14261; (*b*) A. C. McKinlay, B. Xiao, D. S. Wragg, P. S. Wheatley, I. L. Megson and R. E. Morris, *J. Am. Chem. Soc.*, 2008, **130**, 10440; (*c*) P. Horcajada, C. Serre, G. Maurin, N. A. Ramsahye, F. Balas, M. Vallet-Regí, M. Sebban, F. Taulelle and G. Férey, *J. Am. Chem. Soc.*, 2008, **130**, 6774; (*d*) P. Horcajada, C. Serre, M. Vallet-Regi, M. Sebban, F. Taulelle and G. Férey, *Angew. Chem., Int. Ed.*, 2006, **45**, 5974.

4 (*a*) T. Uemura, N. Yanai and S. Kitagawa, *Chem. Soc. Rev.*, 2009, **38**, 1228; (*b*) L. Ma, C. Abney and W. Lin, *Chem. Soc. Rev.*, 2009, **38**, 1248; (*c*) J. Y. Lee, O. K. Farha, J. Roberts, K. A. Scheidt, S. B. T. Nguyen and J. T. Hupp, *Chem. Soc. Rev.*, 2009, **38**, 1450; (*d*) F. Schrôder, D. Esken, M. Cokoja, M. W. E. van den Berg, O. I. Lebedev, G. van Tendeloo, B. Walaszek, G. Buntkowsky, H. H. Limbach, B. Chaudret and R. A. Fischer, *J. Am. Chem. Soc.*, 2008, **130**, 6119; (*e*) Y. K. Hwang, D. Y. Hong, J. S. Chang, S. H. Jhung, Y. K. Seo, J. Kim, A. Vimont, M. Daturi, C. Serre and G. Fèrey, *Angew. Chem., Int. Ed.*, 2008, **47**, 4144; (*f*) M. H. Alkordi, Y. L. Liu, R. W. Larsen, J. F. Eubank and M. Eddaoudi, *J. Am. Chem. Soc.*, 2008, **130**, 12639; (*g*) M. J. Ingleson, J. P. Barrio, J. Bacsa, C. Dickinson, H. Park and M. J. Rosseinsky, *Chem. Commun.*, 2008, 1287; (*h*) F. Gándara, B. Gornez-Lor, E. Gutiérrez-Puebla, M. Iglesias, M. A. Monge, D. M. Proserpio and N. Snejko, *Chem. Mater.*, 2008, **20**, 72; (*i*) S. Hasegawa, S. Horike, R. Matsuda, S. Furukawa, K. Mochizuki, Y. Kinoshita and S. Kitagawa, *J. Am. Chem. Soc.*, 2007, **129**, 2607; (*j*) R. Q. Zou, H. Sakurai and Q. Xu, *Angew. Chem., Int. Ed.*, 2006, **45**, 2542.

5 (*a*) M. Kurmoo, *Chem. Soc. Rev.*, 2009, **38**, 1353; (*b*) L. M. C. Beltran and J. R. Long, *Acc. Chem. Res.*, 2005, **38**, 325; (*c*) J. Ribas, A. Escuer, M. Monfort, R. Vicente, R. Cortes, L. Lezama and T. Rojo, *Coord. Chem. Rev.*, 1999, **193–195**, 1027; (*d*) X. Y. Wang, Z. M. Wang and S. Gao, *Chem. Commun.*, 2008, 281; (*e*) E. Pardo, R. Ruiz-Garcia, J. Cano, X. Ottenwaelder, R. Lescouezec, Y. Journaux, F. Lloret and M. Julve, *Dalton Trans.*, 2008, 2780; (*f*) Q. X. Jia, Y. Q. Wang, Q. Yue, Q. L. Wang and E. Q. Gao, *Chem. Commun.*, 2008, 4894; (*g*) J. R. Li, Q. Yu, E. C. Sanudo, Y. Tao, W. C. Son and X. H. Bu, *Chem. Mater.*, 2008, **20**, 1218; (*h*) C. Biswas, P. Mukherjee, M. G. B. Drew, C. J. Gomez-Garcia, J. M. Clemente-Juan and A. Ghosh, *Inorg. Chem.*, 2007, **46**, 10771; (*i*) J. S. Miller, *Dalton Trans.*, 2006, 2742; (*j*) D. Maspoch, D. Ruiz-Molina and J. Veciana, *J. Mater. Chem.*, 2004, **14**, 2713; (*k*) W. Fujita and K. Awaga, *J. Am. Chem. Soc.*, 2001, **123**, 3601.

6 (*a*) F. A. A. Paz, J. Klinowski, S. M. F. Vilela, J. P. C. Tomé, J. A. S. Cavaleiro and J. Rocha, *Chem. Soc. Rev.*, 2012, **41**, 1088–1110; (*b*) D. J. Tranchemontagne, Z. Ni, M. O'Keeffe and O. M. Yaghi, *Angew. Chem., Int. Ed.*, 2008, **47**, 5136–5147; (*c*) S. Kitagawa, R. Kitaura and S.-i. Noro, *Angew. Chem., Int. Ed.*, 2004, **43**, 2334; (*d*) K. Biradha, Y. Hongo and M. Fujita, *Angew. Chem., Int. Ed.*, 2000, **39**, 3843.

7 (*a*) K. C. Stylianou, R. Heck, S. Y. Chong, J. Bacsa, J. T. A. Jones, Y. Z. Khimyak, D. Bradshaw and M. J. Rosseinsky, *J. Am. Chem. Soc.*, 2010, **132**, 4119; (*b*) A. G. Wong-Foy, O. Lebel and A. J. Matzger, *J. Am. Chem. Soc.*, 2007, **129**, 15740; (*c*) M. Eddaoudi, J. Kim, N. Rosi, D. Vodak,

J. Wachter, M. O'Keeffe and O. M. Yaghi, *Science*, 2002, **295**, 469–472.

8 (*a*) M. Plabst and T. Bein, *Inorg. Chem.*, 2009, **48**, 4331; (*b*) J. M. Taylor, A. H. Mahmoudkhani and G. K. H. Shimizu, *Angew. Chem., Int. Ed.*, 2007, **46**, 795; (*c*) O. R. Evans, D. R. Manke and W. B. Lin, *Chem. Mater.*, 2002, **14**, 3866.

9 (*a*) S. Shimomura, M. Higuchi, R. Matsuda, K. Yoneda, Y. Hijikata, Y. Kubota, Y. Mita, J. Kim, M. Takata and S. Kitagawa, *Nat. Chem.*, 2010, **2**, 633; (*b*) B. F. Hoskins and R. Robson, *J. Am. Chem. Soc.*, 1990, **112**, 1546.

10 (*a*) Y. Takashima, V. M. Martinez, S. Furukawa, M. Kondo, S. Shimomura, H. Uehara, M. Nakahama, K. Sugimoto and S. Kitagawa, *Nat. Commun.*, 2011, **2**, 168; (*b*) M. Dinca, A. Dailly, C. Tsay and J. R. Long, *Inorg. Chem.*, 2008, **47**, 11.

11 (*a*) H. Deng, S. Grunder, K. E. Cordova, C. Valente, H. Furukawa, M. Hmadeh, F. Gándara, A. C. Whalley, Z. Liu, S. Asahina, H. Kazumorio, M. O'Keeffe, O. Terasaki, J. F. Stoddart and O. M. Yaghi, *Science*, 2012, **336**, 1018; (*b*) J. Kim, B. Chen, T. M. Reineke, H. Li, M. Eddaoudi, D. B. Moler, M. O'Keeffe and O. M. Yaghi, *J. Am. Chem. Soc.*, 2001, **123**, 8239.

12 J. M. Tanski, E. B. Lobkovsky and P. Wolczanski, *J. Solid State Chem.*, 2000, **152**, 130.

13 V. A. Blatov, *IUCr CompComm Newsletter*, 2006, **7**, 4–38.

14 (*a*) M. Henry, *ChemPhysChem*, 2002, **3**, 561; (*b*) M. Henry, *ChemPhysChem*, 2002, **3**, 607; (*c*) M. Henry and M. W. Hosseini, *New J. Chem.*, 2004, **28**, 897–906; (*d*) D. R. Turner, M. Henry, C. Wilkinson, G. J. McIntyre, S. A. Mason, A. E. Goeta and J. W. Steed, *J. Am. Chem. Soc.*, 2005, **127**, 11063; (*e*) C. Carpanese, S. Ferlay, N. Kyritsakas, M. Henry and M. W. Hosseini, *Chem. Commun.*, 2009, 6786; (*f*) M. Henry, in *Advances in Quantum Chemical Bonding Structures*, ed. M. V. Putz, Transworld Research Network, Kerala, India, 2009, pp. 153–211; (*g*) H. Senouci, B. Millet, C. Volkringer, C. Huguenard, F. Taulelle and M. Henry, *C. R. Chim.*, 2010, **13**, 69; (*h*) M. Henry, in *Encyclopedia of Nanoscience and Nanotechnology*, ed. H. S. Nalwa, American Scientific Publishers, 2011, vol. 14, pp. 1–43; (*i*) D. M. Weekes, N. Baradel, N. Kyritsakas, P. Mobian and M. Henry, *Eur. J. Inorg. Chem.*, 2012, 5701.

15 (*a*) A. J. Berresheim, M. Müller and K. Müllen, *Chem. Rev.*, 1999, **99**, 1747; (*b*) K. Tsubaki, K. Takaishi, D. Sue and T. Kawabata, *J. Org. Chem.*, 2007, **72**, 4238; (*c*) S. K. Dayal and K. N. Rao, *Indian J. Chem.*, 1967, **5**, 122; (*d*) W. Heitz and R. Ullrich, *Makromol. Chem.*, 1966, **98**, 29; (*e*) W. Z. Heldt, *J. Org. Chem.*, 1965, **30**, 3897–3902; (*f*) H. O. Wirth, K. H. Gönner, R. Stück and W. Kern, *Makromol. Chem.*, 1963, **63**, 30; (*g*) F. Ullmann, *Justus Liebigs Ann. Chem.*, 1904, **332**, 38.

16 (*a*) D. L. Gin, V. P. Conticello and R. H. Grubbs, *J. Am. Chem. Soc.*, 1992, **114**, 3167; (*b*) C. S. Marvel and G. E. Hartzell, *J. Am. Chem. Soc.*, 1959, **81**, 448; (*c*) D. R. McKean and J. K. Stille, *Macromolecules*, 1987, **20**, 1787.

17 H. Lohaus, *Justus Liebigs Ann. Chem.*, 1935, **516**, 295.

18 T. Yamamoto, Y. Hayashi and A. Yamamoto, *Bull. Chem. Soc. Jpn.*, 1978, **51**, 2091.

19 (*a*) N. Miyaura and A. Suzuki, *Chem. Rev.*, 1995, **95**, 2457; (*b*) N. Iwadate and M. Suginome, *J. Organomet. Chem.*, 2009, **694**, 1713; (*c*) J. T. S. Ishikawa and K. Manabe, *Chem. Commun.*, 2008, 3829; (*d*) S. Ishikawa and K. Manabe, *Chem. Lett.*, 2007, **36**, 1302; (*e*) S. Ishikawa and K. Manabe, *Chem. Commun.*, 2006, 2589; (*f*) S. Ishikawa and K. Manabe, *Chem. Lett.*, 2006, **35**, 164; (*g*) J. T. Ernst, O. Kutzki, A. K. Debnath, S. Jiang, H. Lu and A. D. Hamilton, *Angew. Chem., Int. Ed.*, 2002, **41**, 278; (*h*) M. W. Read, J. O. Escobedo, D. M. Willis, P. A. Beck and R. M. Strongin, *Org. Lett.*, 2000, **2**, 3201; (*i*) V. Hensel and A. D. Schlüter, *Chem.–Eur. J.*, 1999, **5**, 421; (*j*) A. J. Blake, P. A. Cooke, K. J. Doyle, S. Gair and N. S. Simpkins, *Tetrahedron Lett.*, 1998, **39**, 9093; (*k*) P. Liess, V. Hensel and A. D. Schlüter, *Justus Liebigs Ann. Chem.*, 1996, 1037; (*l*) P. Galda and M. Rehahn, *Synthesis*, 1996, 614; (*m*) J. J. S. Lamba and J. M. Tour, *J. Am. Chem. Soc.*, 1994, **116**, 11723; (*n*) W. Cheng and V. Snieckus, *Tetrahedron Lett.*, 1987, **28**, 5097.

20 (*a*) *Beilstein Handbuch der Organischen Chemie*, ed. B. Prager, P. Jacobsen, P. Schmidt and D. Stern, Springer Verlag, Berlin, 1923, vol. 6, p. 1164; (*b*) *Beilstein Handbuch der Organischen Chemie*, ed. F. Richter, Springer Verlag, Berlin, 1931, vol. 6 (I supplement), p. 573; (*c*) *Beilstein Handbuch der Organischen Chemie*, ed. F. Richter, Springer Verlag, Berlin, 1944, vol. 6 (II supplement), p. 1129.

21 A. De Silva and C. K. Ober, *J. Mater. Chem.*, 2008, **18**, 1903.

22 I. B. J. Berlman, *Chem. Phys.*, 1970, **52**, 5616.

23 N. I. Nijegorodov, W. S. Downey and M. B. Danailov, *Spectrochim. Acta, Part A*, 2000, **56**, 783–795.

24 I. B. Berlman, *J. Phys. Chem.*, 1970, **74**, 3085.

25 (*a*) M. O. Sinnokrot and C. D. Sherrill, *J. Phys. Chem. A*, 2003, **107**, 8377; (*b*) Y. Zhao and D. G. Truhlar, *J. Phys. Chem. A*, 2005, **109**, 8377; (*c*) Y. Ding, Y. Mei, J. Z. H. Zhang and F. M. Tao, *J. Comput. Chem.*, 2007, **29**, 275–279.

26 (*a*) K. K. Arora, M. S. Talwelkar and V. R. Pedireddi, *New J. Chem.*, 2009, **33**, 57–63; (*b*) K. K. Arora and V. R. Perireddi, *Cryst. Growth Des.*, 2005, **5**, 1309.

27 (*a*) G. R. Desiraju, R. Thaimattam, D. S. Reddy, F. Xue, T. C. W. Mak and A. Nangia, *New J. Chem.*, 1998, **22**, 143; (*b*) D. S. Reddy, D. C. Craig and G. R. Desiraju, *J. Am. Chem. Soc.*, 1996, **118**, 4090.

28 (*a*) C. B. Caputo, V. N. Vukotic, N. M. Sirizzotti and S. J. Loeb, *Chem. Commun.*, 2011, **47**, 8545; (*b*) I. Eryazici, O. K. Farha, O. C. Compton, C. Stern, J. T. Hupp and S. T. Nguyen, *Dalton Trans.*, 2011, **40**, 9189.

29 (*a*) D. Boils, M.-È. Perron, F. Monchamp, H. Duval, T. Maris and J. Wuest, *Macromolecules*, 2004, **37**, 7351; (*b*) P. Brunet, E. Demers, T. Maris, G. D. Enright and J. D. Wuest, *Angew. Chem., Int. Ed.*, 2003, **43**, 5303.

30 J.-H. Fournier, T. Maris, J. D. Wuest, W. Guo and E. Galoppini, *J. Am. Chem. Soc.*, 2003, **125**, 1002.

31 Y. Kawakami, Y. Sakuma, T. Wakuda, T. Nakai, M. Shirasaka and Y. Kabe, *Organometallics*, 2010, **29**, 3281.

32 D. Laliberté, T. Maris and J. D. Wuest, *Can. J. Chem.*, 2004, **82**, 386.

33 S. Basavoju, S. Aitipamula and G. R. Desiraju, *CrystEngComm*, 2004, **6**, 120.

34 (*a*) T. Qin, G. Zhou, H. Scheiber, R. E. Bauer, M. Baumgarten, C. E. Anson, E. J. W. List and K. Müllen, *Angew. Chem., Int. Ed.*, 2008, **47**, 8292; (*b*) R. E. Bauer, V. Enkelmann, U. M. Wiesler, A. J. Berresheim and K. Müllen, *Chem.–Eur. J.*, 2002, **8**, 3858.

35 N. Malek, T. Maris, M. Simard and J. D. Wuest, *Acta Crystallogr., Sect. E: Struct. Rep. Online*, 2005, **61**, o518.

36 B. Sarma and A. Nangia, *CrystEngComm*, 2007, **9**, 628.

37 R. Thaimattam, F. Xue, J. A. R. P. Sarma, T. C. W. Mak and G. R. Desiraju, *J. Am. Chem. Soc.*, 2001, **123**, 4432.
38 (*a*) W. Guo, E. Galoppini, R. Gilardi, G. I. Rydja and Y.-H. Chen, *Cryst. Growth Des.*, **3**, 2001; (*b*) E. Galoppini and R. Gilardi, *Chem. Commun.*, 1999, 173.
39 J.-H. Fournier, T. Maris, M. Simard and J. D. Wuest, *Cryst. Growth Des.*, 2003, **3**, 535.
40 A. L. Spek, *PLATON, A Multipurpose Crystallographic Tool*, Utrecht University, Utrecht, The Netherlands, 2001.
41 L. M. Wilson and A. C. Griffin, *J. Mater. Chem.*, 1993, **3**, 991.

